Large-scale hydraulic conductivities inferred from three-dimensional groundwater flow and ^{4}He transport modeling in the Carrizo aquifer, Texas

Delphine Patriarche and Maria Clara Castro
Department of Geological Sciences, University of Michigan, Ann Arbor, Michigan, USA

Patrick Goblet
Ecole des Mines de Paris, Centre d'Informatique Géologique, UMR 7619 Sisyphe, Fontainebleau, France

Received 11 May 2004; revised 24 August 2004; accepted 1 September 2004; published 13 November 2004.

[1] Through a series of groundwater flow and ^{4}He transport simulations, this study illustrates the conceptual and practical gains achieved by expanding a two-dimensional (2-D) model to a true 3-D one through an application in the Carrizo aquifer and surrounding formations in southwestern Texas. The 3-D simulations allow for a more detailed and accurate definition of the heterogeneities of the system by specifically identifying and differentiating processes that directly impact the three-dimensional hydraulic conductivity field. It is shown that while hydraulic conductivity decreases exponentially along the regional groundwater flow direction, such decrease is better described as a function of depth rather than recharge distance. This relationship reflects the combined influences of differential compaction of the media as well as downdip lithological change. The intrinsic permeability derived from this relationship agrees with field information and with previous findings obtained for the continental crust for depths $\leq$2 km, suggesting that for large scales, decrease rate of permeability with depth is independent of the media. Results also suggest that the solution for groundwater flow simulations based on calibration of hydraulic heads depends on the ratio between hydraulic conductivities of different formations, indicating that an infinite number of solutions are available for calibration of 3-D groundwater flow models. Understanding how geological processes directly affect the 3-D hydraulic conductivity field at the regional scale is essential not only to hydrogeological applications but also at improving our understanding of the Earth's crust and mantle dynamics by allowing for a more accurate quantification of helium and heat fluxes. *INDEX TERMS:* 1040 Geochemistry: Isotopic composition/chemistry; 1829 Hydrology: Groundwater hydrology; 1832 Hydrology: Groundwater transport; 5114 Physical Properties of Rocks: Permeability and porosity; *KEYWORDS:* three-dimensional modeling, hydraulic conductivity, helium 4 crustal flux

Citation: Patriarche, D., M. C. Castro, and P. Goblet (2004), Large-scale hydraulic conductivities inferred from three-dimensional groundwater flow and ^{4}He transport modeling in the Carrizo aquifer, Texas, *J. Geophys. Res.*, *109*, B11202, doi:10.1029/2004JB003173.

1. Introduction

[2] Hydrodynamic parameters in sedimentary groundwater systems vary both at a local and regional scale as a result of geological processes over time. These include deposition, deformation, compaction, and diagenesis, which control the geometry and texture of sedimentary deposits and lead to heterogeneities of the media at all scales [*Koltermann and Gorelick*, 1996; *Le Gallo et al.*, 1998; *Bitzer*, 1999; *de Marsily et al.*, 2002; *Gouze and Coudrain-Ribstein*, 2002].

[3] Because hydraulic conductivity controls both the magnitude and the direction of water velocity [*de Marsily*, 1986] and because it varies over at least 13 orders of magnitude in sedimentary basins, from 10^{-1} m s^{-1} in gravel [*Freeze and Cherry*, 1979] to 10^{-14} m s^{-1} in argillite [*Boisson et al.*, 2001], it is by far the most critical parameter controlling groundwater flow and solute transport. Thus proper description of the internal properties of a groundwater system requires an accurate knowledge of the three-dimensional hydraulic conductivity field.

[4] Direct and indirect measurements of hydraulic conductivity are commonly performed [e.g., *Bredehoeft and Papadopulos*, 1980; *de Marsily*, 1986; *Wierenga et al.*, 1991; *Neuzil*, 1994], providing information on the magnitude of this parameter at the local scale (tens of centimeters to hundreds of meters). In contrast, direct information on hydraulic conductivities at regional scales

0148-0227/04/2004JB003173$09.00

of tens to hundreds of kilometers is unavailable. Numerous approaches have been proposed for generating maps of hydraulic property distributions as inputs to numerical models of groundwater flow and mass transport [e.g., *Carrera and Neuman*, 1986; *Lavenue and Pickens*, 1992; *Harvey and Gorelick*, 1995; *de Marsily et al.*, 2000]. Alternatively, hydraulic conductivity maps are generated through analytical and/or numerical models that attempt to reflect the geological structure of the area [*Bredehoeft et al.*, 1983; *Wei et al.*, 1990; *Castro et al.*, 1998a, 1998b; *Castro and Goblet*, 2003a]. Hydraulic conductivities are obtained, in this case, through calibration on measured hydraulic heads and/or tracer concentrations.

[5] Despite the inherent difficulties of constraining groundwater flow models and accurately defining the hydraulic conductivity field at large scales, such models are critical to a number of important applications. These include assessment and management of groundwater resources, planned hazardous waste disposal projects, and paleoclimatic reconstruction through noble gases [e.g., *Stute et al.*, 1992; *Castro et al.*, 2000; *Castro and Goblet*, 2003b] which requires improving groundwater chronologies. In addition, knowledge of 3-D hydraulic conductivity fields at the regional scale is critical to a better understanding of the Earth's crust and mantle dynamics through a more accurate quantification of helium and heat fluxes [e.g., *O'Nions and Oxburgh*, 1983; *Torgersen and O'Donnell*, 1991]. For example, reconstruction of original $^3He/^4He$ source values in groundwater is required for a correct estimation of He crustal and mantle fluxes. These, in turn, are directly dependent on the groundwater dynamics [see *Castro*, 2004].

[6] Most regional groundwater flow studies have been conducted through 2-D representations, by assuming that flow takes place essentially along two directions, horizontally in the aquifers, vertically in aquitards. In a real groundwater flow system, however, flow is a 3-D process. A critical question that has not yet been addressed in detail is the degree to which 2-D models can adequately represent a 3-D system. How accurately can a 2-D model describe the hydraulic conductivity and thus permeability in a 3-D domain? What are the magnitudes of potential errors introduced by 2-D models, how these might affect flow and transport model results, and to what extent does a 2-D model properly account for mixing of water where flow is three-dimensional?

[7] Through a series of simulations of groundwater flow and ^4He transport, this study aims to answer these questions and illustrate the conceptual and practical gains achieved by expanding a 2-D model to a true 3-D one through an application in the Carrizo aquifer and surrounding formations in southwestern Texas.

2. Geological Background

[8] The Carrizo aquifer, a major groundwater flow system in Texas, is part of a thick regressive sequence of terrigenous clastic sediments that formed within fluvial, deltaic and marine depositional systems in the Rio Grande Embayment area of south Texas on the northwestern margin of the Gulf Coast Basin (Figure 1a).

[9] In the study area comprising mainly Atascosa, McMullen, Frio, and Live Oak counties (Figure 1b), the

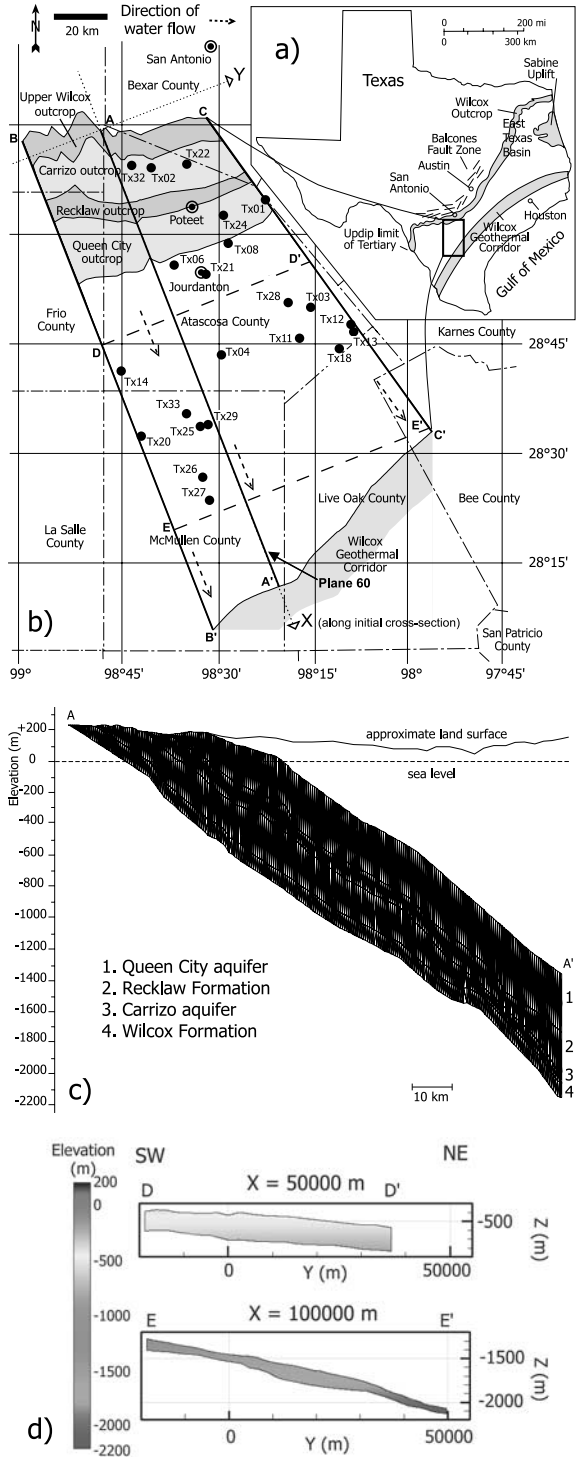

Figure 1. (a) Location and tectonic setting of the study area in Texas after *Hamlin* [1988]. (b) Detailed representation of the study area and delineation of the region covered by the 3-D model. Lateral boundaries of the 3-D model (BB′ and CC′), cross sections DD′ and EE′, 50 and 100 km away from point A, as well as cross section AA′ of *Castro and Goblet* [2003a] shown as bold black lines; locations of ^4He samples shown as solid circles. (c) Simplified representation of plane 60 (3-D model) along AA′. (d) Cross sections DD′ and EE′ through the Carrizo aquifer where a steeper dip of the formation as well as a decrease in thickness is apparent to the east.

Tertiary units in question consist, from base to top, of the undifferentiated Lower Wilcox and lower portion of the Upper Wilcox, the Carrizo, the Recklaw, and the Queen City formations. Sandstones of the Carrizo aquifer make up the uppermost part of the Wilcox Group [*Murray*, 1955; *Fisher*, 1969; *Bebout et al.*, 1978]. The Carrizo lies unconformably on the lower part of the Upper Wilcox, and downdip it contains an increasing amount of shales and mudstones (Figures 1b and 1c). The Carrizo contains more than 90% sandstone in the outcrop areas, but this percentage drops downdip (basinward) to as little as 20%. This trend is more accentuated in the northern part of McMullen County and the northeastern area of Live Oak County but is absent at the boundary between the two counties. The thickness of the Carrizo aquifer is also highly variable, ranging from 50 m in the southern part of McMullen County to about 350 m in the northern part of Live Oak County.

[10] The Lower Wilcox Formation is characterized by thick, laminated organically rich mudstones interbedded with thin laminated argillaceous sand, arenaceous shale and massive clay. The lower part of the Upper Wilcox Formation together with the Lower Wilcox, are over 600 m thick near their outcrop areas, and reach 2400 m in thickness at depths greater than 3 km.

[11] The Recklaw Formation, a confining layer primarily composed of shale, fine sand, and marine mudstone, conformably overlies the Carrizo aquifer. This formation is overlain by the Queen City aquifer, characterized in the area by well-developed, thick coastal barrier sands (Figure 1c). Hydrogeological information on the Recklaw and the Queen City formations is scarce.

[12] The Carrizo and surrounding formations largely crop out in the northern part of Atascosa and Frio counties (Figure 1b). They crop out subparallel to the present-day coastline along a southwest-northeast striking band (Figure 1a) and dip to the southeast. Average dip of the Carrizo aquifer is 1.05°, 1.20° and 1.52° along BB′, AA′, and CC′, respectively (Figures 1b and 1d). The Carrizo aquifer terminates at a major 32 km wide growth fault system (Figures 1a and 1b) commonly known as the Wilcox Geothermal Corridor [*Bebout et al.*, 1978]. These growth faults mark an abrupt increase in thickness and dip of the Wilcox Group. Strong subsidence along these faults resulted in the deposition of thick sections of sand and mud and the isolation of these units, which prevented lateral escape of pore fluids during subsequent compaction. Smaller faults are also found in Atascosa, McMullen, Frio, and Live Oak counties.

[13] Rainfall recharges the Carrizo aquifer in its outcrop area, and groundwater flows basinward to the southeast. Discharge occurs by cross-formational upward leakage, and along fault-related permeability pathways [*Hamlin*, 1988; *Castro and Goblet*, 2003a].

3. Modeling Tool and Governing Equations

[14] To model groundwater flow and mass transport in three dimensions, two classical equations are solved. For incompressible fluids, the general 3-D diffusion equation is expressed as [*de Marsily*, 1986]

$$\nabla \cdot \left(\overline{\overline{K}} \nabla h \right) = S_s \frac{\partial h}{\partial t} + q \qquad (1)$$

where $\overline{\overline{K}}$ is the hydraulic conductivity tensor (L T^{-1}), h is the hydraulic head (L), S_s is the specific storage coefficient (L^{-1}), q is a source term (T^{-1}) representing the amount of fluid withdrawn or added (if negative) per unit volume of porous media, and t is the time (T).

[15] To account for advection, kinematic dispersion, and molecular diffusion, the 3-D transport equation to be solved is expressed as

$$\nabla \cdot \left(\left(\overline{\overline{D}} + \omega \overline{\overline{d}} \right) \nabla C - C\mathbf{U} \right) = \omega \frac{\partial C}{\partial t} + qm \qquad (2)$$

where $\mathbf{U}$ is the Darcy velocity (L T^{-1}), $\overline{\overline{d}}$ is the pore diffusion coefficient tensor (L^2 T^{-1}) of the solute in question, ω is the porosity, qm (M L^{-3} T^{-1}) is a source term corresponding to the added or withdrawn mass of tracer per unit volume and per unit of time, and C (mol m^{-3}) is the concentration of solute in water. $\overline{\overline{D}}$ is the dispersivity coefficient tensor (L^2 T^{-1}) expressed as $\overline{\overline{D}} = \overline{\overline{\alpha}} U$, where $\overline{\overline{\alpha}}$ is the (diagonal) dispersivity tensor (L) described by three components, one along the direction of velocity (α_L), and two transversal (perpendicular) to the direction of the flow (α_T). The latter are taken equal.

[16] All 3-D simulations for fluid flow and mass transport were conducted with the finite element code METIS (Modélisation des Ecoulements et des Transferts avec Interaction en milieu Saturé) [*Cordier and Goblet*, 1999] in steady state conditions.

4. Systematics and Overview of ^{4}He Behavior in Groundwater Systems

[17] Because of its conservative nature, ^{4}He is transported in and by water without reacting with the reservoir rocks. Typically, ^{4}He is present in the mantle (primordial origin), in the crust (radiogenic origin) and in the atmosphere (as a consequence of the degassing of the Earth). These components of different origins present specific characteristics, which allow for identification of their sources and sinks [e.g., *Craig et al.*, 1978; *Allegre et al.*, 1987; *Martel et al.*, 1989; *Ballentine et al.*, 1991]. The concentration of ^{4}He in groundwater frequently exceeds that expected for water in solubility equilibrium with the atmosphere (air-saturated water, ASW). Commonly, most of the ^{4}He excesses in old groundwater have a radiogenic origin where ^{4}He results from α decay of natural U and Th present in many common rocks in the crust. In groundwater systems, these excesses can result either from in situ production (taking place within the groundwater system) or have an external origin, from deeper layers or from the crystalline basement [e.g., *Torgersen and Clarke*, 1985; *Castro et al.*, 1998a, 1998b]. In the latter case, ^{4}He must be transported upward through advection, dispersion and/or diffusion. A mantle component of ^{4}He might also be present.

[18] Previous work on the Carrizo aquifer in the study area [cf. *Stute et al.*, 1992; *Castro et al.*, 2000] (Figure 1b and Table 1) show excesses of ^{4}He concentrations as compared to ASW values of up to 2 orders of magnitude. These excesses increase with distance from the outcrop as well as with depth, reflecting the incorporation of radiogenic and/or mantle ^{4}He that is progressively added to recharge water entering with an atmospheric ^{4}He

Table 1. Helium Isotope Concentrations for Samples Collected in the Carrizo Aquifer Used for Comparison With Calculated Concentrations From Transport Model Simulations[a]

Well Sample	Distance,[b] km	Elevation Above Sea Level, m	^{4}He, 10^{-6} mol m^{-3}
TX 01	17.3	−156.8	3.694
TX 02	3.1	154.0	2.052
TX 03	48.9	−901.7	42.56
TX 04	54.3	−787.0	17.13
TX 06	28.9	−302.7	3.882
TX 08	26.5	−252.0	26.55
TX 11	55.2	−988.5	44.17
TX 12	54.8	−1146.1	104.5
TX 13	57.2	−1175.0	106.5
TX 14	56.2	−572.9	28.11
TX 18	61.3	−1159.8	104.4
TX 20	72.1	−942.5	55.05
TX 21	32.4	−430.4	5.488
TX 22	4.4	137.0	2.954
TX 24	19.7	−211.0	12.54
TX 25	76.4	−1063.5	74.11
TX 26	85.0	−1219.5	200.9
TX 27	90.5	−1318.0	265.8
TX 28	45.8	−802.7	21.19
TX 29	74.9	−1050.1	80.57
TX 32	2.2	153.0	3.034
TX 33	70.5	−1122.9	53.18
ASW (18°C)[c]			2.010

[a]See *Castro et al.* [2000]. The name of well samples is indicated as well as its distance to the Carrizo outcrop in the 3-D model and its elevation above sea level.

[b]From origin of Carrizo outcrop in the 3-D model.

[c]After *Stute et al.* [1992]. The ^{4}He concentration for air-saturated water (water in solubility equilibrium with the atmosphere) at 18°C is also indicated for comparison.

component. These excesses are mostly of radiogenic origin and result partly from in situ production, partly from external sources [*Phillips and Castro*, 2003; *Castro*, 2004].

5. The 3-D Model Construction

5.1. Determining Lateral Boundaries of the Domain

[19] Groundwater flow and ^{4}He transport were simulated in a 2-D model comprising the Lower Wilcox, Carrizo, Recklaw, and Queen City formations (adapted from *Castro and Goblet* [2003a]; see Figure 1c), which assumed that regional groundwater flow direction in Atascosa and McMullen counties (AA′, Figure 1b) was perpendicular to the lines of equal water age, as defined by *Pearson* [1966].

[20] Here, we adopt a similar methodology in simulating groundwater flow and ^{4}He transport in a 3-D system. The surface area therefore includes the 22 wells in the Carrizo aquifer where ^{4}He and all other noble gases have been analyzed [*Stute et al.*, 1992; *Castro et al.*, 2000] (Figure 1b and Table 1). Two natural boundaries delimit this 3-D domain; these are the outcrop of the Lower Wilcox Formation to the north and the growth fault system to the south. Because no natural lateral hydrogeological boundaries exist, the lateral boundaries of the 3-D model domain (BB′ and CC′, Figure 1b) were taken to be perpendicular to the distribution of equipotential lines. Such a selection allows imposition of a null water flux along these boundaries. As it will be seen later, the orientation of equipotential lines in the Queen City aquifer is similar to that of the Carrizo aquifer and thus justifies the imposition of a null flux along the entirety of the lateral boundaries. The geostatistical procedure used to determine the distribution of equipotential lines in the Carrizo aquifer and in the recharge area of the Lower Wilcox is described below.

5.1.1. Hydraulic Head Data

[21] Historical records (1930 to present) of water levels in the Carrizo aquifer were gathered from various reports [*Lonsdale*, 1935; *Turner*, 1936; *Anders*, 1957, 1960; *Anders and Baker*, 1961; *Harris*, 1965; *Alexander and White*, 1966] and from the Texas Water Development Board (Ground-water database, 2003, available at http://www.twdb.state.tx.us/publications/reports/GroundWaterReports/GWDatabaseReports/GWdatabaserpt.htm). Hydraulic heads obtained from these records are heterogeneously distributed in space and in time. A total of 224 hydraulic head records were used to determine the distribution of equipotential lines in the Carrizo aquifer. Because of extensive well development, in particular since 1956, significant withdrawals have occurred in the area, inducing the presence of a nonsteady state regime. To reconstruct hydraulic head values prior to that extensive exploitation, corrections based on available information on annual drawdowns [*Alexander and White*, 1966] were applied to original hydraulic head measurements made in wells in the confined portion of the Carrizo aquifer. For wells located in the outcrop area, corrections applied were based on the mean distance of the water table to land surface based on records of wells where drawdowns were negligible. In the Lower Wilcox where there is a scarcity of records, only eleven hydraulic head measurements in the outcrop area were used (see auxiliary material[1]).

5.1.2. Geostatistical Modeling

[22] Distribution of equipotential lines in the Carrizo aquifer and recharge area of the Lower Wilcox (Figure 2) was obtained through a geostatistical analysis of available hydraulic head measurements performed with the ISATIS code [*Bleines et al.*, 2002]. Unlike classical interpolators such as moving average and inverse distance, geostatistics "tailor" the estimation process according to the structure of the spatial correlation between hydraulic head measurements. After this spatial correlation structure (covariance or variogram) has been identified from the available data, the estimation can be shown to be optimal.

[23] Hydraulic head measurements were considered as random draws of a regionalized variable H (a function of space), which can be treated as a random one [*Matheron*, 1973]. The variogram $\gamma(h) = \frac{1}{2}\mathrm{Var}[H(x+h) - H(x)]$ of H expresses its intrinsic spatial variability at a distance h between two points.

[24] Exploratory analysis of the available 235 hydraulic head measurements shows that the entire data set is relatively heterogeneous. The variogram analysis shows that the limit of $\gamma(h)$ with increasing distance h is not constant, strongly suggesting a nonstationary behavior of H. Thus a nonstationary geostatistical modeling was performed in order to fit the hydraulic head measurements and to determine the distribution of equipotential lines. One of the solutions consists in fitting a generalized covariance [*de Marsily et al.*, 2000] of order κ (rather than a variogram), where κ designates the degree of the polynomial drift which

[1]Auxiliary material is available at ftp://ftp.agu.org/apend/jb/2004JB003173.

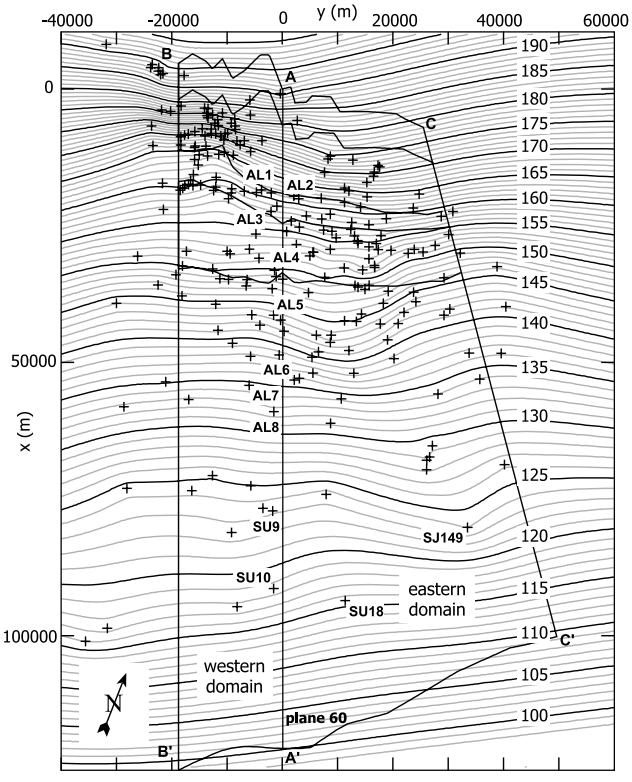

Figure 2. Distribution of equipotentials in the Carrizo aquifer and outcrop of the Lower Wilcox obtained through geostatistical modeling performed on 235 hydraulic head measurements. Lateral no-flow boundaries BB′ and CC′ are essentially perpendicular to the equipotential lines.

suits the representation of the global behavior of the variable H [e.g., *Matheron*, 1973; *Kitanidis*, 1993].

[25] Hydraulic head distribution was obtained through intrinsic kriging [*Matheron*, 1973] using this geostatistical model. The distribution of equipotential lines in the entire domain (Figure 2) was then used to define the direction of the vertical planes forming the lateral boundaries (BB′ and CC′, Figure 1b) of the 3-D model.

5.2. Expansion of a 2-D Model Into a 3-D One

[26] In order to compare 2-D and 3-D model results and to assess the extent to which a more accurate representation of the hydraulic conductivity field is obtained through 3-D simulations as compared to 2-D ones, construction of the 3-D model was achieved by successively projecting an initial 2-D model (cross section AA′, see Figure 1c, adapted from *Castro and Goblet* [2003a]) along the Y direction, transverse to AA′ (Figure 1b). The 3-D model represents the exact topography of the different formations [*Harris*, 1965; *Alexander and White*, 1966; *Payne*, 1972a, 1972b; *Klemt et al.*, 1976], both at the surface (outcrop areas) and at depth. In addition, with the exception of the Lower Wilcox, all the observed variations in thickness in all formations are incorporated in the 3-D model. Because the Lower Wilcox is extremely thick, it is represented here with a constant thickness of 100 m. This is of no consequence because the transmissivity is expected to be extremely small due to the very low permeability of this sequence (e.g., *Brinkman*, 1981).

[27] The original 2-D model [*Castro and Goblet*, 2003a] is composed of triangles uniformly distributed over the entire length of the cross section with length sizes of 50 m, except near four minor faults and one major fault representing the Wilcox Geothermal Corridor where the grid is refined. In order to minimize both memory requirements and CPU time while conducting 3-D simulations, the original 2-D mesh was modified using the code DELOS [*Stab*, 1995] in order to reduce the total number of elements. Specifically, the four minor faults were removed as it was concluded that their impact on groundwater flow and ^{4}He transport is negligible [*Castro and Goblet*, 2003a]. The modified 2-D mesh is composed of 80 m long triangles along X (Figure 1b) uniformly distributed over the entire length of the cross section, except near the major growth fault system, where the grid is refined. Element length size was maximized by ensuring that the accuracy of results was preserved and that results were indistinguishable from those obtained with the original 2-D mesh under similar boundary conditions. The new 2-D mesh (along AA′, Figure 1b) comprises 21,908 triangular elements and 31 monodimensional segments.

[28] The 3-D model is composed of pentahedrals built with analogous triangles joining two successive 2-D planes as described above, as well as rectangles obtained through two analogous segments in the growth fault system. The 3-D model totals 233 planes which are identified by their number, from 1 to 233, i.e., from BB′ toward CC′; the original 2-D model corresponds to plane 60. The 3-D model covers a surface of $\sim$7000 km^2 (Figure 1b), and it includes 5,089,848 elements.

6. Boundary Conditions, Calibration Data, and Parameter Values

6.1. Groundwater Flow Simulations

[29] Hydraulic heads were imposed on the outcrop areas of all four formations as well as on top of the confined Queen City aquifer in a step-by-step procedure through geostatistical modeling. For the Queen City aquifer, few historical records of hydraulic head are available (see the auxiliary material). Corrections applied to some hydraulic head measurements were done in a similar manner to that previously described for the Carrizo aquifer. To obtain the distribution of hydraulic heads at the top of the Queen City, a geostatistical modeling procedure similar to that described above for the Carrizo aquifer and Wilcox Formation was carried out. Simultaneously, a hydraulic head of 100 m was imposed at the end of plane AA′, in order to respect the average hydraulic gradient of $\sim 3 \times 10^{-4}$ observed in the area. The resulting distribution of equipotentials in the Queen City shows a regional direction of fluid flow very similar to that observed in the Carrizo, upon which the orientation of external lateral boundaries was based. The obtained hydraulic head values were then retrieved at each node of the top of the aquifer.

[30] Hydraulic head values were subsequently extracted at all nodes located at the boundaries Carrizo/Recklaw and Queen City/Recklaw, respectively. Additional geostatistical modeling on this extracted data set was performed using a generalized covariance model, in order to ensure the hydraulic continuity in the domain [*Tóth*, 1995; *Kitanidis*,

1999]. Hydraulic head values were then obtained at all nodes on the outcrop of the Recklaw Formation.

[31] Hydraulic head values from the three different geostatistical simulations were then combined into one set and imposed on the outcrop areas of all formations as well as on top of the confined Queen City aquifer.

[32] Because of the significant thickness and impermeable nature of the Wilcox Formation [*Brinkman*, 1981], a no-flow boundary condition was imposed at its base. A no-flow boundary condition was also imposed at the external lateral boundaries of the domain. In addition, a hydraulic conductivity of 10^{-5} m s^{-1} was prescribed to the elements representing the growth fault system, the southern boundary of the domain. This condition, together with an imposed hydraulic head at the top of the Queen City, allows the water to flow upward, mimicking the groundwater behavior in this area.

[33] Previous sensitivity tests have shown that groundwater flow in the Carrizo aquifer is essentially dictated by its hydraulic conductivity and that of the overlying confining Recklaw Formation [*Castro and Goblet*, 2003a]. The following discussion will thus center on possible hydraulic conductivity values for these two formations. Hydraulic conductivities for the Queen City aquifer and for the Wilcox Formation were taken to be 5×10^{-5} and 10^{-11} m s^{-1}, respectively [*Castro and Goblet*, 2003a].

[34] For all simulations, hydraulic conductivities (unknown parameter) of the Carrizo and Recklaw formations were obtained through calibration of the model on measured hydraulic heads available in the confined portion of the Carrizo aquifer within the 3-D domain (a total of 149 measurements).

6.2. The ^{4}He Transport Simulations

[35] For the ^{4}He transport simulations, all 22 samples (Figure 1b and Table 1) in the study area were used. Given tortuosities of the media, a ^{4}He diffusion coefficient of 1.33×10^{-9} m^2 s^{-1} was taken for the Carrizo and Queen City aquifers, and 6.65×10^{-10} m^2 s^{-1} for the Recklaw Formation [*Castro and Goblet*, 2003a, 2003b]. All simulations were conducted with a longitudinal (α_L) and two transversal (α_T) dispersivity coefficients of 125 and 12.5 m, respectively [*Castro and Goblet*, 2003a]. Average porosity values used are 20, 12.5, 35, and 26% for the Queen City, Recklaw, Carrizo and Wilcox formations, respectively [e.g., *Castro and Goblet*, 2003a].

[36] A ^{4}He concentration of 2.01×10^{-6} mol m^{-3} (corresponding to that of ASW at a temperature of 18°C) was imposed on outcrop areas. On top of the Queen City aquifer, an outlet condition was prescribed, which allows ^{4}He to be evacuated by advection to the overlying layers. A flux of ^{4}He representing the external contribution (crust + mantle), was imposed at the base of the Carrizo aquifer. This upward flux value is our calibration parameter for the transport model. Inside the domain, and as calculated by *Castro et al.* [2000], a source term representing the in situ production was imposed to all nodes.

7. Hydraulic Conductivity Versus Recharge Distance

[37] The primary goal of this study is to compare results from 2-D and 3-D groundwater flow and transport models in order to assess the adequacy of a 2-D model at representing a real three-dimensional system. Specifically, we are interested in learning how accurately a 2-D model captures the 3-D hydraulic conductivity field of a real (three-dimensional) domain. Are there features directly affecting the hydraulic conductivity and thus the intrinsic permeability field of a regional groundwater flow system that are not apparent in 2-D simulations? We will demonstrate: (1) the inadequacy of expressing hydraulic conductivity variations as a function of recharge distance in 3-D representations, (2) the ability of a hydraulic conductivity-depth relationship to better describe the 3-D groundwater flow system, and (3) the impact of lateral facies change (along Y) on the 3-D hydraulic conductivity field. As it will be seen, features 2 and 3 are not readily identified in 2-D models.

7.1. Testing the Hydraulic Conductivity Field Structure of a 2-D Model Versus a 3-D One

[38] *Castro and Goblet* [2003a] concluded that the regional distribution of hydraulic heads in this region is best explained by an exponential decrease of hydraulic conductivities with increased recharge distance, both in the Carrizo and Recklaw formations, given by

$$K_c = 5 \times 10^{-4} \exp(-d_c/12{,}000)$$
$$K_r = 3 \times 10^{-8} \exp(-d_r/12{,}000), \quad (3)$$

where d_c and d_r represent distances (m) of any point from the origin of the Carrizo and Recklaw outcrop areas, respectively. Initial hydraulic conductivities for the Carrizo and Recklaw are 5×10^{-4} and 3×10^{-8} m s^{-1}, respectively. Here, we investigate the suitability of this hydraulic conductivity-recharge distance relationship for reproducing the distribution of measured hydraulic heads in the entire 3-D domain. By applying the same relation and boundary conditions in the 3-D model, we now test the robustness of this relation previously obtained with the 2-D model.

[39] Results of 3-D groundwater flow simulations (open squares, Figure 3a) show that although measured and calculated hydraulic heads are well correlated ($r^2 = 0.957$), calculated values are biased and fall below line 1:1. It should be noted that r^2 [*Davis*, 2002] expresses the degree of linearity, but gives no information on bias. A perfect linearity does not imply a perfect fit, as a systematic bias of calculated values with respect to measured ones might be present. The average deviation between calculated and measured values is evaluated through the mean squared error

$$\mathrm{MSE} = \frac{1}{n}\sum_{1}^{n}\left|\frac{V_{\mathrm{calculated}} - V_{\mathrm{measured}}}{V_{\mathrm{measured}}}\right|^2,$$

n being the number of measurements considered, the mean relative error (MRE), where

$$\mathrm{MRE} = \frac{1}{n}\sum_{1}^{n}\left|\frac{V_{\mathrm{calculated}} - V_{\mathrm{measured}}}{V_{\mathrm{measured}}}\right|,$$

as well as the mean absolute error,

$$\mathrm{MAE} = \frac{1}{n}\sum_{1}^{n}\left|V_{\mathrm{calculated}} - V_{\mathrm{measured}}\right|.$$

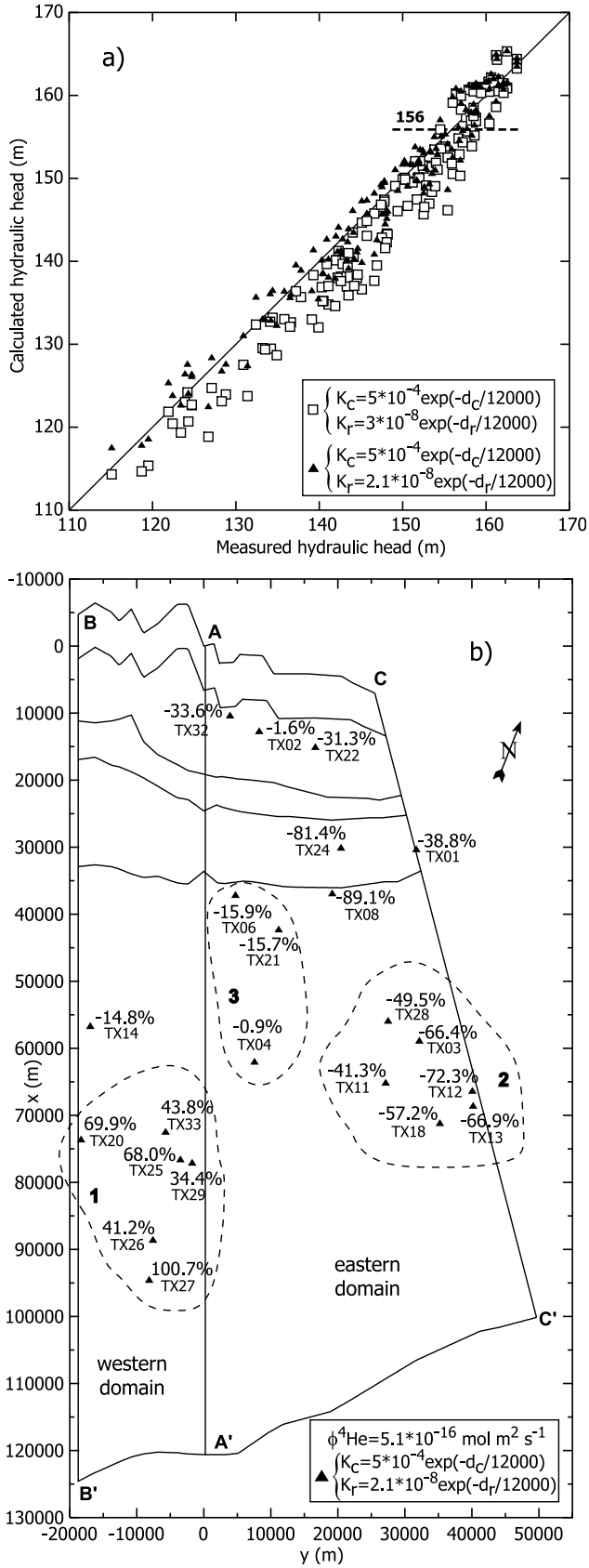

Figure 3. (a) Calculated hydraulic heads (m) plotted as a function of measured ones for hydraulic conductivities expressed as a function of recharge distance using relation (3) for an initial hydraulic conductivity of the Recklaw K_r of 3×10^{-8} m s^{-1} (open squares) and K_r of 2.1×10^{-8} m s^{-1} (solid triangles). Line 1:1 is plotted for reference. (b) Map view of the domain with location of ^{4}He samples (solid triangles). Deviations (%) between calculated and measured ^{4}He concentrations under groundwater flow conditions are as presented in Figure 3a (solid triangles) using an external ^{4}He flux (ϕ^4He) of 5.1×10^{-16} mol m$^{-2}_{rock}$ s^{-1}.

[40] The 3-D simulation results show clearly that calculated hydraulic heads $\leq$156 m are underestimated (Figure 3a), reaching a maximum error of -6.2% at well SJ149 located the farthest from the outcrop area in the eastern part of the domain (Figure 2). Similarly, calculated hydraulic heads at wells AL1 through AL8, SU9 and SU10 (Figure 2), located near plane 60 (AA′) and used for calibration of the 2-D model, are also underestimated in the 3-D model.

[41] It is important to know if slight differences in hydraulic heads, obtained through a linear interpolation in the 2-D model and a geostatistical approach in the 3-D model, might give rise to these discrepancies. To this end, we conducted a 2-D simulation along plane 60 using the same hydraulic heads along this plane as those imposed on the 3-D model. In a similar manner of results obtained by *Castro and Goblet* [2003a], 2-D simulations conducted here display no bias and show that a good calibration was achieved, with maximum and minimum deviations of +1.97% and -1.67%, respectively. Such results show that the observed bias displayed by the 3-D model does not result from slight differences on imposed hydraulic heads, but rather is related to the solution of the three-dimensional problem.

7.2. Groundwater Flow and Transport Simulations on the 3-D Model

7.2.1. Calibration of Hydraulic Head Measurements and ^{4}He Transport Analysis

[42] We proceeded to eliminate the bias on calculated hydraulic heads by calibrating the 3-D groundwater flow model as a function of recharge distance. Calibration was achieved (Figure 3a, solid triangles) by modifying only the initial hydraulic conductivity of the Recklaw Formation, from 3×10^{-8} m s^{-1} to 2.1×10^{-8} m s^{-1}. Although this change results in only a slight improvement of $r^2 = 0.963$, the goodness of fit, evaluated through the MSE improved considerably by dropping from 6.7 to 2.4, while the MRE decreased from 2.0% to 1.3% (MAE = 1.86 m).

[43] Multiple calibrated and unbiased scenarios on hydraulic heads for the 3-D model are possible. By choosing to present here this particular scenario, and keep the same hydraulic conductivity field within the Carrizo while operating a minor change within the above confining layer allows us to assess the deviations in place between measured and calculated ^{4}He concentrations.

[44] The ^{4}He transport simulations were conducted with the external ^{4}He flux of 5.1×10^{-16} mol m$^{-2}_{rock}$ s^{-1}, derived by *Castro and Goblet* [2003a]. Results show clearly that distribution of ^{4}He concentrations obtained through the

3-D model is not accurately reproduced in the entire domain (Figure 3b). In particular, three main subregions may be distinguished in the confined portion of the Carrizo (Figure 3b). Subregion 1, in the western portion of the domain, exhibits generally overestimated calculated concentrations with respect to measured ones, up to +100.7% with a high MRE of 59.7%. Subregion 2, in the eastern portion of the domain, exhibits generally underestimated calculated concentrations (up to −72.3%), with a high MRE of 58.9%. Wells in subregion 3, located in the central portion of the domain exhibit a fairly good calibration, with a maximum deviation of −15.9% and a low MRE of 10.8%. Samples located in the northeastern part of Atascosa County (TX08, TX24, and to some extent TX01) as well as sample TX14 display a somewhat marginal behavior. These will be discussed later (see section 9.6), together with samples located in the recharge area.

7.2.2. Model Calibration for Fluid Flow and ^{4}He Transport in Subregions of the Domain

[45] Given the spatial ^{4}He concentration distribution discrepancies in the 3-D model, we focused on independently calibrating ^{4}He concentrations in subregions 1 and 2 by changing the hydraulic conductivity fields of the Carrizo and the Recklaw formations, while assuming an unchanged ^{4}He flux. In both groundwater flow scenarios, calibration was achieved by changing the rate of change of hydraulic conductivities with increased recharge distance within these two formations.

[46] Calibration of ^{4}He concentrations in subregion 1 is rather good, with MRE = 10.7%, and maximum and minimum deviations of −16.9% and +13.6%, respectively. Calculated hydraulic heads display a very similar coefficient of determination ($r^2 = 0.963$) as compared to the previously calibrated model (see section 7.2.1), as well as very similar MSE (2.4) and MRE (1.3%) errors. While calibration of the transport model was achieved on subregion 1, fit for subregions 2 and 3 has worsen considerably.

[47] Attempts to calibrate ^{4}He concentrations for subregion 2 failed. Best fit is given for MRE = 24.3%, while deviations ranges up to +50.1%. Simultaneously, concentrations in subregions 1 and 3 are now largely overestimated (e.g., MRE = 478.6% on subregion 1). Once again, a good calibration on calculated hydraulic heads was obtained ($r^2 = 0.961$, MSE = 2.7).

7.3. Implications for Hydraulic Conductivity Variations

[48] Results show that expressing hydraulic conductivities as a function of recharge distance in a three-dimensional system, as well as in a two-dimensional one, is suitable to correctly represent the distribution of hydraulic heads. It also becomes apparent that a multitude of head calibrated 3-D groundwater flow scenarios can be easily obtained with multiple three-dimensional hydraulic conductivity fields. In contrast, 3-D representation of hydraulic conductivities as a function of recharge distance is not suitable for reproducing the distribution of ^{4}He concentrations.

[49] Two other parameters that directly impact the distribution of ^{4}He concentrations in groundwater systems are the ^{4}He derived from in situ production and ^{4}He derived from underlying units (external flux). It should be noted that ^{4}He production rates employed for all simulations were estimated using U and Th concentrations measured in the Carrizo reservoir rocks (see *Castro et al.*, 2000). As extensively discussed by *Castro and Goblet* [2003a], there is no evidence for major lithologic changes in rocks/minerals producing most of the ^{4}He in the Carrizo, and particularly between subregions 1 and 2 of the domain. In addition, sensitivity tests conducted on the 3-D calibrated groundwater flow model (Figure 3a, see section 7.2.1) show that flux variations of over 2 orders of magnitude between subregions 1 and 2 would be required to reproduce ^{4}He concentrations, and there is no geological evidence to explain such a strong flux variation between these two subdomains.

[50] One main such spatial characteristic in this 3-D domain is a much steeper basinward dip of formations in the eastern part of the region (Figures 1b and 1d). *Castro et al.* [2000] concluded that ^{4}He concentrations are well correlated with recharge distance as well as with depth, and that accumulation of ^{4}He in groundwater is also directly correlated with water velocity and therefore hydraulic conductivity and intrinsic permeability. This suggests that a hydraulic conductivity-depth relation might be better suited to represent the ^{4}He concentrations distribution in the 3-D domain and thus be better suited to represent the three-dimensional groundwater flow system.

8. Hydraulic Conductivity Versus Depth

[51] Many geological and geochemical processes contribute to a decrease in hydraulic conductivity with depth. For example, compaction generally results in porosity loss as a result of grain rearrangement [*Athy*, 1930; *Terzaghi and Peck*, 1967]. Theoretical models [*Gangi*, 1978], in situ measurements [*Revil and Cathles*, 2002], and laboratory results [*Morrow et al.*, 1994] suggest that permeability generally decreases with increasing confining effective stress. In response to increased temperature and pressure, physical compaction is also generally accompanied by cementation and other diagenetic and hydrogeochemical changes that affect water flow paths [*Land et al.*, 1987; *Connolly et al.*, 1990].

[52] While a number of studies [*Brace*, 1984; *Manning and Ingebritsen*, 1999; *Saar and Manga*, 2004] have focused on assessing changes in permeability at a scale of the continental crust without considering lithological changes, regional studies of the first few kilometers below land surface attempt to incorporate lithofacies variations [e.g., *Fogg*, 1986; *Desbarats et al.*, 2001]. In the absence of a clear understanding or quantitative evaluation of the processes involved in porosity loss with depth, regional-scale studies commonly invoke fairly arbitrary permeability/depth curves derived from a wide range of compaction curves expressing porosity as a function of depth [e.g., *Rowan et al.*, 2003].

[53] In steady state flow modeling, hydraulic conductivity acts to change the magnitude and direction of advective transport, whereas porosity does not play a significant role [*Smith and Schwartz*, 1981]. Therefore, in all simulations presented here, porosity is kept constant in all four formations. Below, we investigate the degree to which change in hydraulic conductivity (K) with depth (z) can reproduce the distribution of ^{4}He concentrations in the 3-D domain.

The discussion that follows will be uniquely centered in the three subregions of the domain (1, 2, and 3, Figure 3b).

8.1. Evidence for Depth-Related Hydraulic Conductivity Variations

[54] It was concluded that the distribution of ^{4}He concentrations could not be represented accurately when expressing a decrease in hydraulic conductivity as a function of recharge distance; concentrations are overestimated in subregion 1 and strongly underestimated in subregion 2 (Figure 3b). Transition between the two takes place at the proximity of plane AA′.

[55] Because hydraulic conductivities along plane AA′ (see section 7.2.1) are similar to those obtained from field information [*Klemt et al.*, 1976; *Mace and Smyth*, 2003], we apply a *K-z* relationship in the 3-D model that respects the initial and final hydraulic conductivity values along AA′. Such relationship is given by

$$K_c = 5 \times 10^{-4} \exp((z - z_c)/244)$$
$$K_r = 2.1 \times 10^{-8} \exp((z - z_r)/261), \quad (4)$$

where z is the altitude (m) at the center of the considered element at a location of interest, and z_c and z_r are the altitudes at the center of all elements of the Carrizo and Recklaw outcrops, respectively, along Y in the 3-D model. Here we use an unchanged ^{4}He flux of 5.1×10^{-16} mol m_{rock}^{-2} s^{-1}. Under these conditions, we are able to compare the response of ^{4}He behavior between an established relationship hydraulic conductivity-recharge distance (see section 7.2.1, Figure 3b), versus hydraulic conductivity-depth.

[56] Hydraulic heads calculated with these assumptions agree well with measured values (r^2 = 0.973, MSE = 1.9, MAE = 1.65 m, Figure 4a). Despite a large remaining bias (MRE = 41.9%, Figure 4b), agreement between calculated and measured ^{4}He concentrations is greatly improved. Indeed, by expressing hydraulic conductivities as a function of depth, subregions of dissimilarity between measured and calculated values are no longer present. Concentrations now display a similar trend in the entire domain with underestimation of all calculated values. In addition, r^2 has also greatly improved (0.966). Because calculated hydraulic conductivities near outcrop areas are in good agreement with field information [*Mace and Smyth*, 2003], this uniform underestimation of ^{4}He concentrations suggests that hydraulic conductivity decreases more rapidly with depth, or that the ^{4}He flux value is higher. We investigate this below.

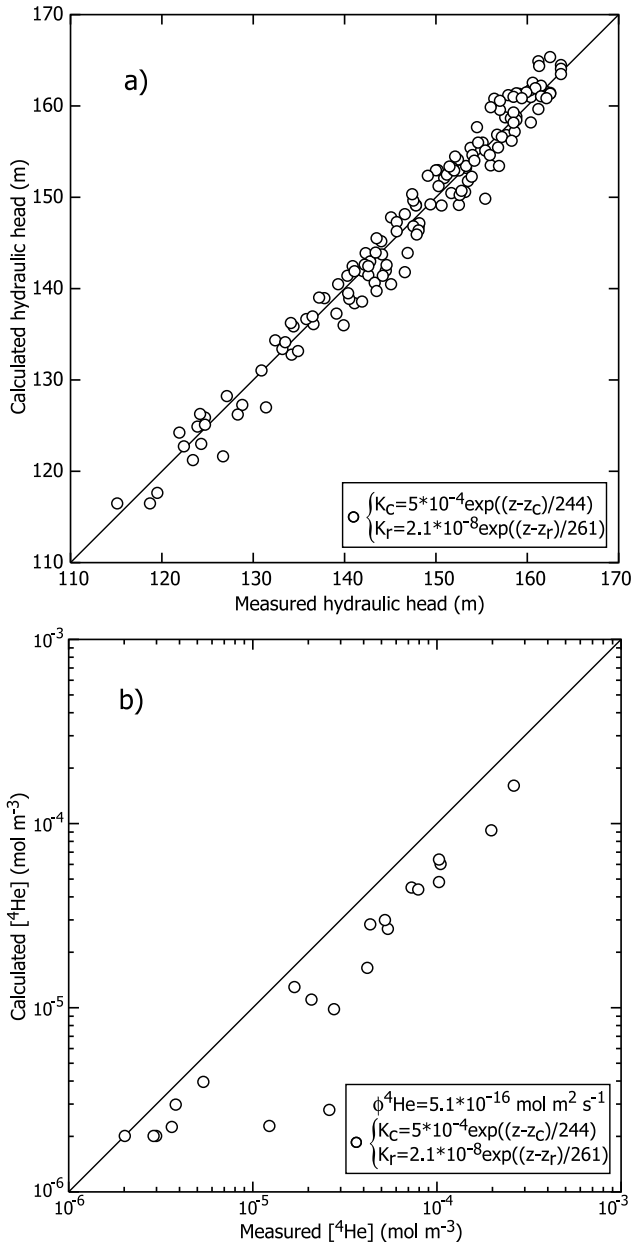

Figure 4. (a) Calculated versus measured hydraulic heads (m) (open circles) where hydraulic conductivities are expressed as a function of depth using relation (4) and same initial hydraulic conductivities as that presented in Figure 3a (solid triangles). (b) Calculated ^{4}He concentrations plotted as a function of measured ones for transport simulations under flow conditions corresponding to relation (4) (Figure 4a) and a ^{4}He flux of 5.1×10^{-16} mol m_{rock}^{-2} s^{-1} (open circles). All calculated concentrations fall below line 1:1 plotted for reference.

8.2. Evaluation of Optimal Parameters to Represent ^{4}He Behavior

8.2.1. The ^{4}He Response to Changes in Hydraulic Conductivity With Depth

[57] A greater decrease rate of hydraulic conductivity with depth in the Carrizo and Recklaw formations was imposed. ^{4}He flux remained unchanged. For example, results of simulations with the following relationship

$$K_c = 5 \times 10^{-4} \exp((z - z_c)/216)$$
$$K_r = 2.1 \times 10^{-8} \exp((z - z_r)/231) \quad (5)$$

show that deviations between measured and calculated values greatly improved as compared to the previous results for most of the deepest samples, where impact on hydraulic conductivity decrease is stronger (e.g., TX27 with a deviation of 15.8% versus 39.3%; TX13 with a deviation of 0.5% versus 43.3%). In contrast, there is little improvement for samples at shallower depths (e.g., TX06, TX21). Sensitivity tests show that even greater decrease rates in hydraulic conductivities with depth yield only a

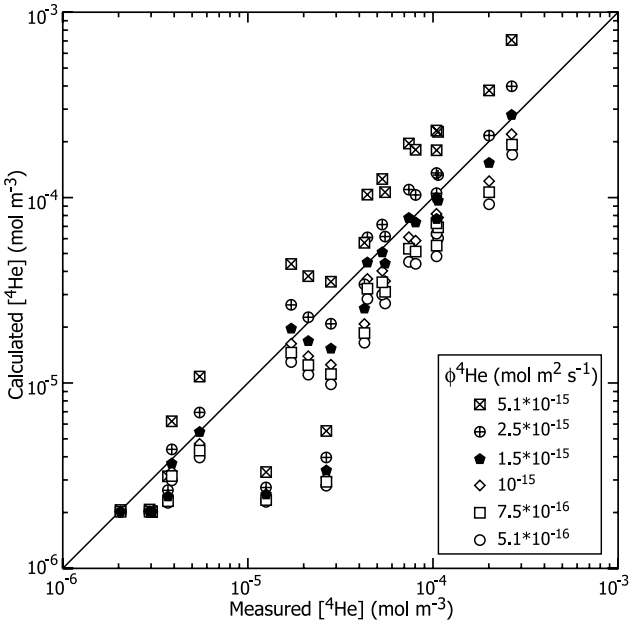

Figure 5. Calculated versus measured ^{4}He concentrations under groundwater flow conditions presented in Figure 4a for fluxes varying from 5.1×10^{-16} to 5.1×10^{-15} mol m_{rock}^{-2} s^{-1}. Results show that the best fit is obtained for a ^{4}He flux of 1.5×10^{-15} mol m_{rock}^{-2} s^{-1} (solid pentagons).

slight improvement on shallower samples, while deeper samples become very strongly overestimated.

8.2.2. The ^{4}He Response to Changes in the External Flux

[58] We have shown that a homogeneous rate of change of hydraulic conductivities with depth does not reduce differences between measured and calculated ^{4}He values at shallower depths. Could these inconsistencies reflect different ^{4}He external flux values under the 3-D hydraulic conductivity field as described in section 8.1 (Figure 4a)? To address this question, sensitivity tests were carried out under these groundwater flow conditions in which ^{4}He external fluxes vary from 5.1×10^{-16} to 5.1×10^{-15} mol m_{rock}^{-2} s^{-1} (Figure 5). Results show that an optimal fit is obtained with a flux value of 1.5×10^{-15} mol m_{rock}^{-2} s^{-1} ($r^2 = 0.960$; MRE = 12.7%), for samples within the three original regions (solid pentagons; Figure 5). However, ^{4}He deviations resulting from this "optimal fit" are unevenly distributed within the three subregions (Figure 6). Although a net bias is no longer present and deviations are much smoother across the region than those derived when hydraulic conductivity is expressed as a function of recharge distance (see section 7.2.1 and Figure 3b), discrepancies remain between the three subregions. Specifically, subregions 1, 2, and 3 display distinct MSE and MRE values of 181.3, 483.8, and 80.7 and 11.1, 17.2, and 6.9%, respectively. Clearly, deviations are much smaller in the central portion of the domain as compared to the lateral regions.

9. Calibration of ^{4}He Transport Model

[59] To further improve the fit between calculated and measured ^{4}He concentrations while applying a uniform rate of hydraulic conductivity change with depth across the region proved unsuccessful. Whenever good agreement was obtained for subregions 1 and 2, differences in subregion 3 would increase. The opposite holds true. These results suggest that another parameter in addition to depth is influencing distribution of hydraulic conductivities within this region. One obvious parameter in this complex depositional system is the lithological composition within each formation; sand content, for example, plays a fundamental role in determining hydraulic conductivities [e.g., *Land et al.*, 1987]. We therefore proceeded to take a closer look at the distribution of sand percentage within the Carrizo aquifer and Recklaw Formation.

9.1. Introducing Lateral Hydraulic Conductivity Changes

[60] Although sand content of the Carrizo aquifer is high (80–100%) and relatively homogeneous in outcrop areas, it decreases downdip to values less than 20% [*Payne*, 1972a]. In contrast, the proximity of plane 84, subregion 3 in the

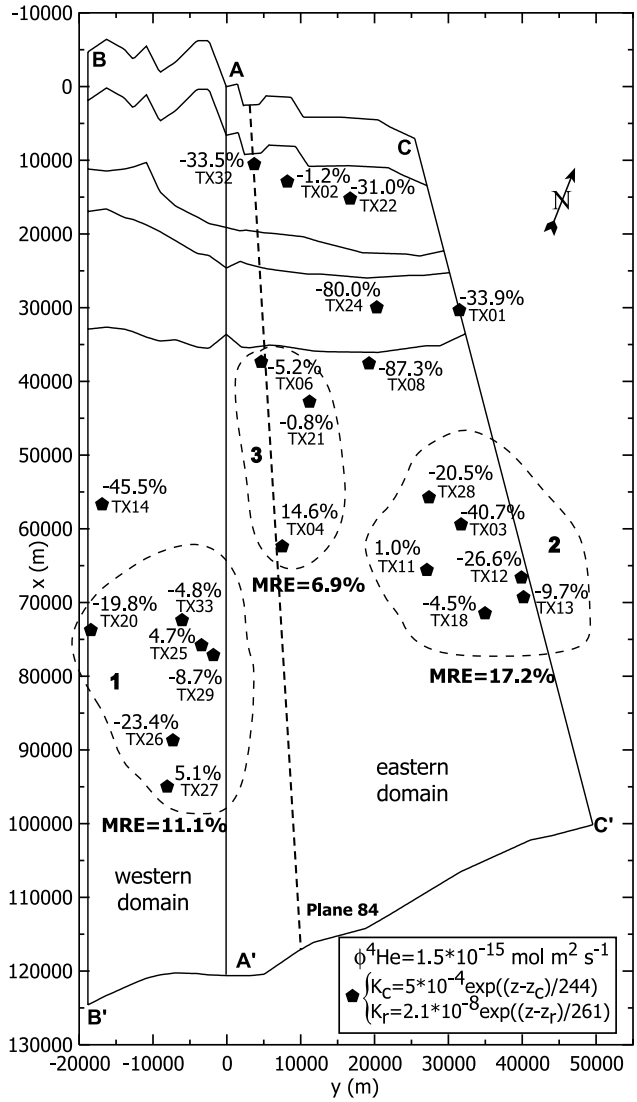

Figure 6. Map view of deviations (%) between measured and calculated ^{4}He concentrations resulting from the best fit (see Figure 5, $\phi^4He = 1.5 \times 10^{-15}$ mol m_{rock}^{-2} s^{-1}).

central portion of the 3-D model (Figure 6) coincides with an area where sand percentage remains over 80% much further from the Carrizo outcrop areas as compared to subregions 1 and 2. This longitudinal sand deposit may be the result of filling of incised channels developed by paleoriver systems [*Payne*, 1972a]. A sand percentage decrease is observed along the Y direction, toward lateral boundaries CC′ and BB′, respectively.

[61] Calibration of the model is attempted by incorporating, in addition to hydraulic conductivity changes along Z, a lateral hydraulic conductivity change along Y. Our departure point at incorporating hydraulic conductivity changes along Y expresses changes of hydraulic conductivity with depth only, as follows:

$$K_c = 5 \times 10^{-4} \exp((z - z_c)/245)$$
$$K_r = 2.1 \times 10^{-8} \exp((z - z_r)/264). \quad (6)$$

This relationship, with an imposed ^{4}He flux of 1.5×10^{-15} mol m_{rock}^{-2} s^{-1}, was the one found that best reproduces ^{4}He concentrations in the central portion of the domain (subregion 3). Only variations within the Carrizo are introduced here. Hydraulic conductivity within the Carrizo (K_c) is expressed as a linear function of y_c, with decreasing values to the east and west of plane 84, respectively, by linear gradient G_c as follows:

$$K_c = 5 \times 10^{-4} \exp((z - z_c)/((G_c(\, y_c - 3778)) + 245))$$
$$K_r = 2.1 \times 10^{-8} \exp((z - z_r)/264), \quad (7)$$

with $G_c = 5.05 \times 10^{-4}$ for $y_c \leq 3778$ m (west of plane 84) and $G_c = -2.69 \times 10^{-4}$ for $y_c > 3778$ m (east of plane 84), where 3778 m corresponds to the y coordinate of plane 84 at the beginning of the Carrizo outcrop (y_c).

[62] Using these parameters, a good agreement with measured hydraulic heads was obtained (MSE = 2.1, MRE = 1.1%). Calculated ^{4}He values also show a significant improvement. Specifically, MSEs for subdomains 1, 2, and 3 dropped to 127.9, 399.1, and 62.8, respectively, as opposed to those of relationship (6) (209.0, 540.0, and 66.9, respectively), where hydraulic conductivity changes are uniquely along Z. MREs now obtained are, for subregions 1, 2, and 3, 10.0, 14.5, and 6.6% respectively. These results show that, although not carrying the same impact as compared to changes as a function of depth, lateral variations of hydraulic conductivity in the Carrizo due to lithological heterogeneities play a nonnegligible role at reproducing the distribution of ^{4}He concentrations. Despite the significant improvement, samples from subregion 2 still yield a relatively high MSE value (e.g., TX03 underestimated by 39.0%). This raises the question as to the influence of sand content variations in the Recklaw Formation.

[63] Analysis of sand content within the Recklaw Formation [*Payne*, 1972b] indicates the presence of major changes particularly within the eastern portion of the 3-D domain. Here, an area with little sand content (0–20%) is largely coincident with subregion 2. Lower sand percentage becomes more dominant toward the eastern lateral boundary of the 3-D model (CC′). Variations in the western part of the domain are much less pronounced. In order to represent major trends of lithological variation in the Recklaw Formation, we proceeded to introduce an additional linear hydraulic conductivity decrease G_r along the Y direction on the eastern domain only, in a similar manner as previously done for the Carrizo. Calibration of the ^{4}He transport model was achieved using the following relations:

$$K_c = 5 \times 10^{-4} \exp((z - z_c)/((G_c(\, y_c - 3778)) + 245))$$
$$K_r = 2.1 \times 10^{-8} \exp((z - z_r)((G_r(\, y_r - 4159)) + 264)), \quad (8)$$

with $G_c = 5.05 \times 10^{-4}$ for $y_c \leq 3778$ m and $G_c = -2.69 \times 10^{-4}$ for $y_c > 3778$ m and $G_r = 0$ for $y_r \leq 4159$ m and $G_r = -1.25 \times 10^{-3}$ for $y_r > 4159$ m, where 4159 m corresponds to the y coordinate on plane 84 at the beginning of the Recklaw outcrop (y_r).

[64] This results in good agreement between calculated and measured hydraulic heads (r^2 = 0.973, MSE = 1.8; MRE = 1.1%; MAE = 1.62 m; Figure 7a). Calibrated ^{4}He concentrations (Figures 7b and 7c), which display indistinguishable MRE values as compared to the previous case, present now a significantly improved MSE of 310.1 as opposed to 399.1 for subregion 2, in addition to a general improved MSE of 192.3 within the three subregions as opposed to 223.4 in the previous case. This set of parameters is the one that best replicates data on hydraulic heads and on ^{4}He concentrations and it thus represents our 3-D calibrated groundwater flow and transport model.

9.2. Intrinsic Permeability Versus Depth

[65] While we have focused our attention at defining as accurately as possible the hydraulic conductivity field in this sedimentary groundwater flow system, it is also of particular relevance to understand how our resulting relationship intrinsic permeability-depth relates, if at all, with previously defined more general permeability-depth relationships for the crust [e.g., *Manning and Ingebritsen*, 1999; *Saar and Manga*, 2004]. One fundamental issue to address is whether or not the observed depth dependency of this parameter is independent of the geological setting in question (e.g., sedimentary, metamorphic, volcanic), and thus valid for the crust as a whole, at least for the first 2 km depth.

[66] In our particular 3-D groundwater flow system where hydraulic conductivity decreases over 4 orders of magnitude with increasing depth, up to ~2 km, such decrease translates by far a decrease of intrinsic permeability k, which describes the properties of the medium alone. Indeed, taking into account the observed temperature increase between the outcrop area (~20°C) and the deepest well where data is available (~70°C) results in a decrease of dynamic viscosity μ by a factor of 2.48, while water density ρ changes are negligible taking into account both, the observed temperature variations and salinity values (0–1 g L^{-1}) within most of the 3-D domain [*Hamlin*, 1988]. Thus, taking these considerations into account and the fact that $k = \mu K/\rho g$, where g is the acceleration of gravity (9.81 m s^{-2}), we have proceeded to determine an approximate relationship k-z for the Carrizo aquifer at the center of our domain (plane 84, Figure 6) for a salinity of 0 g L^{-1} and temperatures of 20°C (ρ = 998.2 kg m^{-3}, $\mu = 1.002 \times 10^{-3}$ Pa s [*de Marsily*, 1986]), and 70°C (ρ = 977.8 kg m^{-3}, $\mu = 0.404 \times$

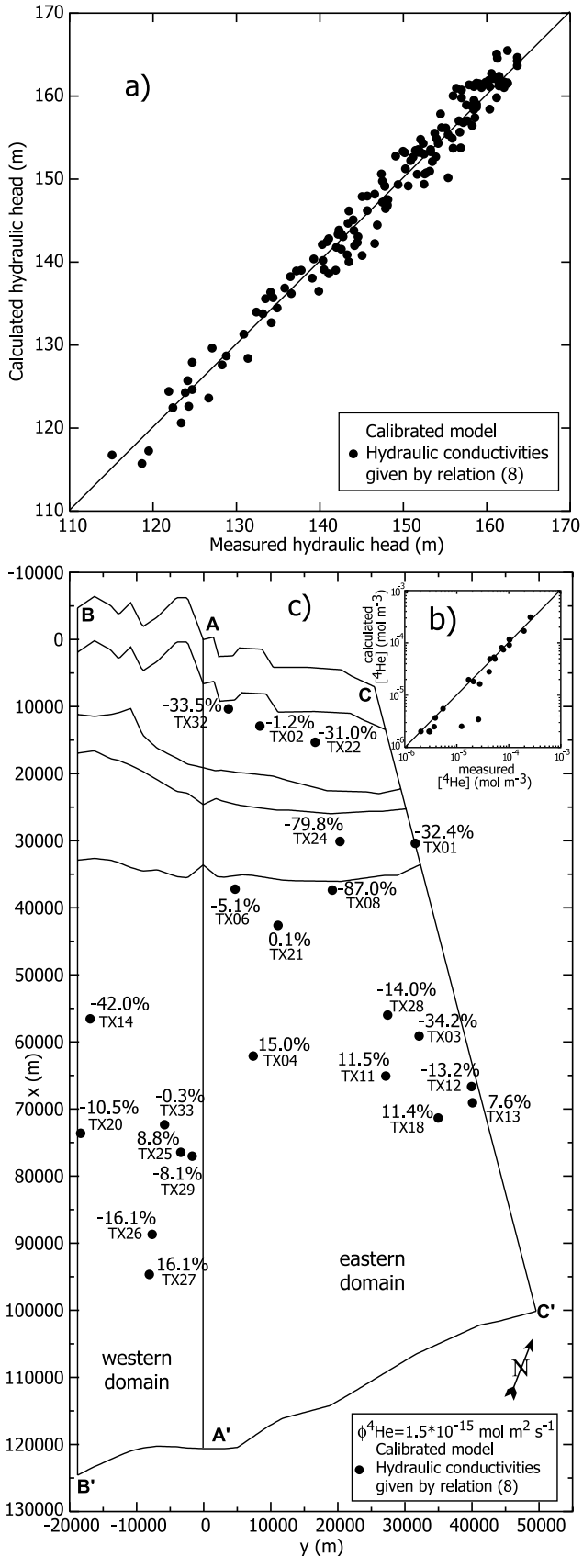

Figure 7. (a) Calibrated groundwater flow obtained with relation (8). Here hydraulic conductivity is expressed simultaneously along Z (as a function of depth) and along Y to incorporate both effects of compaction and lithological facies change. Line 1:1 is plotted for reference. (b) Calibrated ^{4}He transport model using groundwater flow conditions presented in Figure 7a. Calculated versus measured ^{4}He concentrations are shown as solid circles; line 1:1 is plotted for reference. (c) Deviations (%) between calculated and measured ^{4}He concentrations for calibrated transport model (solid circles).

10^{-3} Pa s [*de Marsily*, 1986]), respectively. Our *k-z* relationship for 20 and 70°C are given by $k = 5.1 \times 10^{-11}$ exp(−depth/245), and $k = 2.1 \times 10^{-11}$ exp(−depth/245), respectively, indicating a change by a factor of 2.43 (Figure 8). Of particular relevance is the similarity between our estimated *k-z* relationships and that one proposed by *Saar and Manga* [2004] for the Oregon Cascades volcanic setting for depths up to 2 km expressing the vertical permeability (k_v) as $k_v = 5 \times 10^{-13}$ exp(−depth/250) (Figure 8). Specifically, the similar characteristic lengths (denominator of the exponential term, in meters) found in both studies (i.e., sedimentary versus volcanic setting) suggest that large-scale permeabilities evolve similarly with depth, independently of the type of medium. To account for the presence of stratification in the volcanic ashes of the Cascades and unlike the sandstones of the Carrizo aquifer, *Saar and Manga* [2004] assume the media strongly anisotropic with $k_h/k_v = 10^3$, where k_h is the horizontal permeability. It can be clearly seen that our *k-z* relationship falls approximately at the center of the k_v and k_h curves as determined by *Saar and Manga* [2004] (Figure 8). The same holds true for the curves proposed by *Manning and Ingebritsen* [1999], where *k* varies as a power law of depth (Figure 8), and considering an identical 10^3 anisotropy for the continental crust [see *Saar and Manga*, 2004]. Agreement with results by *Manning and Ingebritsen* [1999] are good for depths up to ∼2,200 m, corresponding to the maximum depth of the Carrizo in our 3-D domain and, particularly, for depths where data for calibration of the 3-D groundwater flow model is available, up to 1425 m (Figure 8). This further reinforces the conclusions reached above.

[67] Although only few in situ permeability measurements are available in the Carrizo aquifer and Wilcox Formation, in particular, in our 3-D domain, it is important to note that such values (A, B, C, and solid circles, see Figure 8) are very close to our calculated intrinsic permeabilities. Downdip (depths >2.2 km), our proposed curve compares with some data from the Wilcox Formation obtained from field tests. However, it departures from the main field data trend by 1−2 orders of magnitude. This is likely due to a lack of calibration data in the deepest part of the model, which results in a weaker constrained hydraulic conductivity and thus permeability field in the deepest portion of the model.

9.3. External Helium Fluxes: Implications for the Earth's Structure

[68] It is important to note that the ^{4}He external flux value of 1.5×10^{-15} mol m_{rock}^{-2} s^{-1} found by accounting for flow

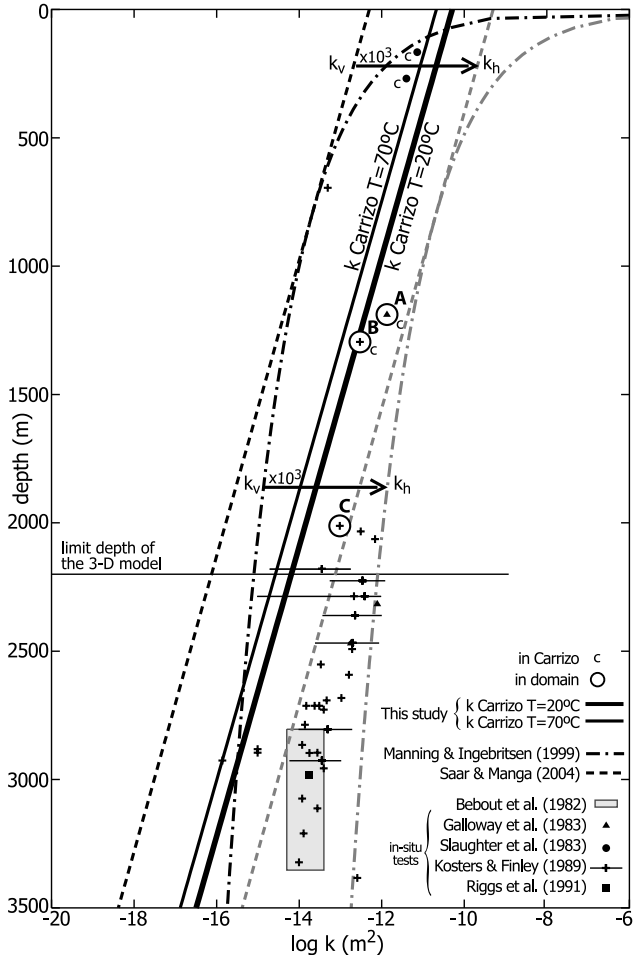

Figure 8. Log permeability (m^2) as a function of depth, plotted for the Carrizo at plane 84 of the 3-D model, considering constant density and dynamic viscosity of the water at $T = 20°C$ (bold solid line) and $T = 70°C$ (thin solid line). Curves for vertical permeabilities (dashed black lines) determined by *Saar and Manga* [2004] and *Manning and Ingebritsen* [1999] are plotted, as well as the corresponding horizontal permeabilities (dashed grey lines) considering an anisotropy of $k_h/k_v = 10^3$. Data points represent the permeability determined from field tests; c indicates data from the Carrizo formation; all others belong to the Wilcox. Open circles (A, B, and C) are located in the 3-D domain.

and transport in three dimensions in the Carrizo aquifer is not representative of the whole terrestrial ^{4}He crustal flux [cf. *O'Nions and Oxburgh*, 1983; *Castro et al.*, 1998a]. This flux value, which is significantly smaller than the latter, represents an intermediate value between the one determined through a very simple analytical model in the Carrizo aquifer ($\sim 5 \times 10^{-15}$ mol m_{rock}^{-2} s^{-1} [*Castro et al.*, 2000]), and that one found through calibration of the original 2-D model ($\sim 5 \times 10^{-16}$ mol m_{rock}^{-2} s^{-1} [*Castro and Goblet*, 2003a]).

[69] Accurate estimation of both crustal and mantle helium fluxes in many continental areas requires a thorough understanding of complex groundwater systems and thus of its hydraulic conductivity field. Indeed, as shown by *Castro et al.* [1998a, 1998b] and *Castro* [2004], deep groundwater fluxes strongly impact and modify both, ^{3}He and ^{4}He fluxes, as well as external R/Ra ratios (R is the groundwater ^{3}He/^{4}He ratio; Ra is the atmospheric ^{3}He/^{4}He ratio) upon which quantification of mantle helium (R/Ra $\sim$ 8 for mid-ocean ridges basalts (MORB) [*Farley and Neroda*, 1998]) contributions are based. Crustal and mantle helium fluxes are reduced due to progressive dilution exerted by recharge water on the original helium crustal and mantle components, while original external R/Ra ratios are also strongly modified by in situ production due to groundwater mixing and diffusion processes. Indeed, tests of the distribution of R/Ra values in the Carrizo aquifer carried out in the 2-D original model [*Castro*, 2004], show that relatively high R/Ra values ($\sim$0.14) entering the aquifer and indicating a mantle He contribution of $\sim$1.5% are quickly lowered by extremely low (0.0025) in situ production ratios almost totally devoid of ^{3}He. Such lessening gives rise to measured "typical crustal" R/Ra values of about 0.055. Further analysis on the R/Ra behavior shows that groundwater R/Ra values between 0.01 and 0.05 (considered as typical crustal values) may be the result of a significant (perhaps dominant) mantle component modified by low ^{3}He/^{4}He in situ production ratios. It further suggests that mantle ^{3}He fluxes might be substantially higher than previously thought. Such observations raise additional questions concerning the mantle structure as proposed by *O'Nions and Oxburgh* [1983], who suggest the presence of a convective upper mantle capable of releasing its small amount of radiogenic heat and helium efficiently, but that is isolated from the lower mantle from which most of the heat lost from the ocean basins is derived. Under this scenario, mantle heat and He fluxes are decoupled, the upper mantle providing all helium flux in the oceans, while supplying only $\sim$5% of the heat.

[70] Similar to previous observations in sedimentary systems [e.g., *Castro et al.*, 1998a, 1998b], and in the Carrizo aquifer in particular [*Castro*, 2004], M. O. Saar et al. (Quantifying magmatic, crustal, and atmospheric helium contributions to volcanic aquifers using all noble gases: Implications for magmatism and groundwater flow patterns, submitted to *Geochemistry, Geophysics, and Geosystems,* 2004, hereinafter referred to as Saar et al., submitted manuscript, 2004) show that interpretation of R/Ra values in continental volcanic areas representative of the MORB without simultaneous consideration of helium concentrations and component mixing, can mask and reduce the inferred magnitude of a mantle/magmatic helium signature in groundwater. Indeed, by taking into account groundwater mixing processes these authors show that the magmatic helium signature on the eastern side of the Oregon Cascades (external R/Ra $\sim$ 5.2) is comparable to the western side, where typically the largest magmatic helium and heat signals are observed [*Ingebritsen et al.*, 1994]. Such observations suggest that mantle/magmatic volatile flux beneath the eastern flanks of the Cascades is comparable to the flux under the western flanks but that mixing with recharge water masks such high magmatic helium fluxes. Such findings are similar in characteristics to *Manga*'s [1998], who found significant but also largely diluted magmatic/mantle heat signals in some cold springs on the east side of the Cascades crest.

[71] Findings by *Castro* [2004] and Saar et al. (submitted manuscript, 2004) suggest the presence of higher mantle helium fluxes than previously thought and the possibility for

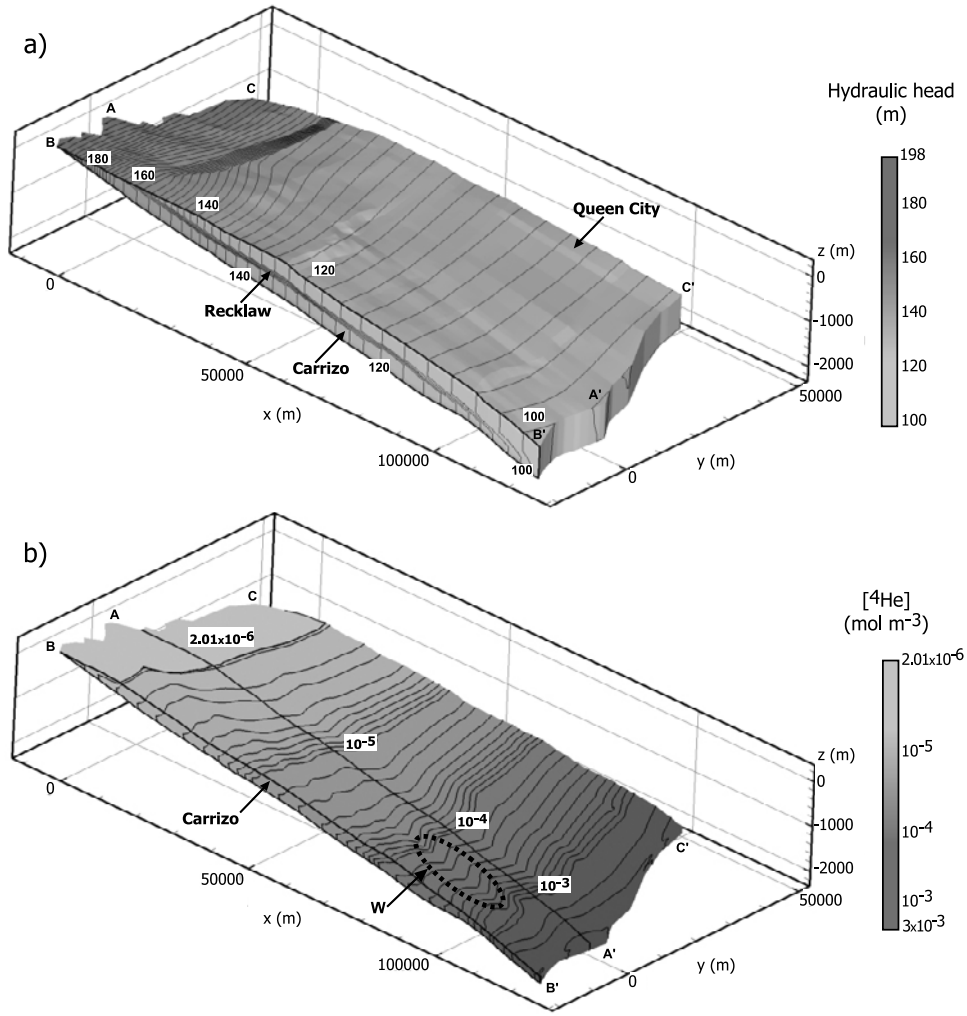

Figure 9. (a) Distribution of calculated hydraulic heads in the calibrated 3-D model. These indicate the presence of an essentially horizontal flow in the Carrizo and Queen City aquifers, and a dominant vertical flow within the Recklaw Formation. (b) Distribution of ^{4}He concentration contours (mol m^{-3}) for the 3-D calibrated transport model within the Carrizo aquifer. Contour lines express constant variations of one unit inside each order of magnitude between 2×10^{-6} and 3×10^{-3} mol m^{-3}; contour values of 2.02×10^{-6}, 2.05×10^{-6}, 1.5×10^{-5}, 1.5×10^{-4}, and 1.5×10^{-3} mol m^{-3} are also indicated.

absence of decoupling between mantle helium and heat transport as previously suggested. This, in turn, would suggest the presence of a more continuous and permeable boundary to helium transport between the upper and lower mantle than that proposed by *O'Nions and Oxburgh* [1983]. By further constraining the three-dimensional hydraulic conductivity field in the Carrizo aquifer and surrounding formations through the set of simulations here presented, we expect to move one step forward at clarifying some of these aspects. Future analysis of heat and ^{3}He transport in this 3-D system will hopefully enhance our understanding of this couple's behavior transport.

9.4. General Functioning of the 3-D Calibrated Groundwater Flow and Transport Model

[72] As previously shown by *Castro and Goblet* [2003a], distribution of calculated hydraulic heads in our 3-D calibrated model (Figure 9a), also indicate an essentially horizontal flow within the Carrizo and Queen City aquifers and vertical flow within the Recklaw Formation. Distribution of hydraulic heads in the 3-D domain, also show that the latter is indirectly recharged by the Carrizo aquifer. As expected, lower hydraulic conductivities are found to the east in the deepest parts of the Carrizo, at the proximity of the growth fault system. Smallest hydraulic conductivities reach 3.1×10^{-8} and 1.4×10^{-12} m s^{-1} for the Carrizo and the Recklaw, respectively, and are close to those found by *Castro and Goblet* [2003a] (3.8×10^{-8} and 6.4×10^{-12} m s^{-1}, respectively).

[73] Infiltration rate integrated over the entire Carrizo outcrop is 197 mm yr^{-1}. This is approximately 30% of net precipitation, which was measured to be 646 mm yr^{-1} in Atascosa County over a 30-year period [*Alexander and White*, 1966]. Such high direct contribution (30%) from precipitation is, however, unlikely. Part of the infiltrated groundwater within the Carrizo aquifer likely results from

direct infiltration from the Atascosa River and all its tributaries, which meander along most of the Carrizo outcrop within the area covered by our 3-D domain.

[74] Concentrations of ^{4}He in the Carrizo aquifer exhibit a 3-order of magnitude increase with depth and recharge distance, from a typical atmospheric value of 2.01×10^{-6} mol m^{-3} in the recharge area up to 3×10^{-3} mol m^{-3} at the proximity of the growth fault system (Figure 9b). Vertical concentration contours throughout the Carrizo aquifer illustrate this progressive increase. Accumulation of ^{4}He due to in situ production as well as contribution from the external flux is not evenly distributed. For example, along the western part of the domain (area W; Figure 9b), increase of ^{4}He takes place at a slower rate. This is due to a smaller thickness of the Recklaw Formation in this area. As the Recklaw thins, the ability of ^{4}He to cross this formation increases, i.e., ^{4}He escapes the Carrizo upward more easily and faster by advection, dispersion and diffusion [see, e.g., *Castro et al.*, 1998a, 1998b].

9.5. Sensitivity of the 3-D Model to Hydraulic Conductivities

[75] Sensitivity tests on hydraulic heads were conducted by increasing and decreasing independently, Carrizo and Recklaw initial hydraulic conductivities (K_c and K_r, respectively) by 1 order of magnitude as compared to the calibrated scenario. Results show that calculated hydraulic heads are very similar for an imposed initial K_c and K_r 1 order of magnitude lower and higher, respectively, and reach a maximum deviation of ~20% (Figure 10a, open circles and pluses, respectively). In a similar manner, calculated hydraulic heads are very close for imposed initial K_c and K_r 1 order of magnitude higher and lower, respectively, reaching a maximum deviation of ~27% (Figure 10a, open squares and crosses, respectively). Such results suggest that the solution for groundwater flow simulations does not depend directly on the hydraulic conductivity field of the Carrizo or Recklaw formations independently, rather it depends on the ratio between these two hydraulic conductivity fields K_c/K_r. Simulations where both initial K_c and K_r are changed simultaneously by 1 order of magnitude (open and solid triangles; Figure 10a) confirms this dependency. This, in turn, and as previously discussed among others by *Konikow and Bredehoeft* [1992], *Maloszewski and Zuber* [1993], and *Castro and Goblet* [2003a], shows that an infinite number of solutions are available for calibration of groundwater flow models.

[76] This universe of reasonable solutions is greatly reduced when ^{4}He concentrations are considered. Sensitivity tests show that ^{4}He concentrations are greatly overestimated (up to 9.5 times) when simultaneously decreasing initial hydraulic conductivity values in the Carrizo and Recklaw formations (Figure 10b). Conversely, when increasing initial hydraulic conductivities 1 order of magnitude in both formations, most samples are largely underestimated (Figure 10b).

9.6. Discussion of Specific ^{4}He Samples

9.6.1. Recharge Area

[77] Samples TX02, TX22, and TX32, located in the Carrizo outcrop area (Figure 7c), were not objects of discussion in this article. Our calibrated 3-D transport model

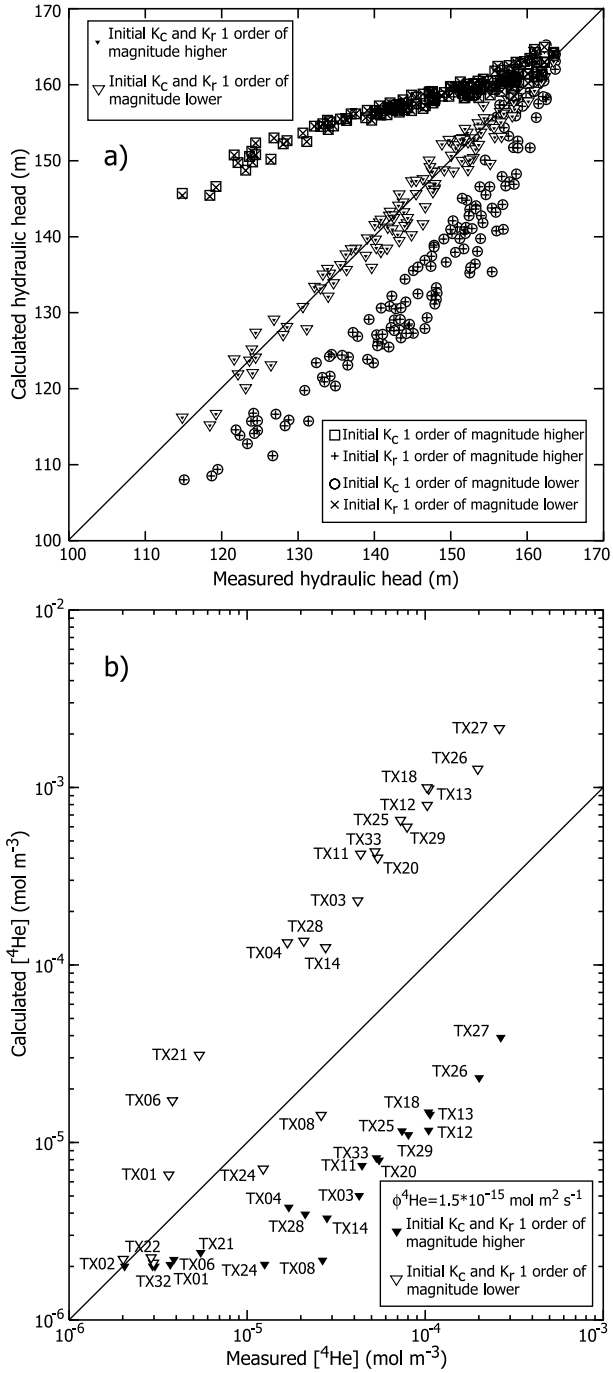

Figure 10. (a) Calculated versus measured hydraulic heads (m). Line 1:1 is plotted for reference; all parameters are the same as those of Figure 7a (calibrated 3-D groundwater flow model) except initial hydraulic conductivity values for the Carrizo aquifer (K_c) and Recklaw Formation (K_r); K_c 1 order of magnitude higher (open squares); K_r 1 order of magnitude higher (pluses); K_c 1 order of magnitude lower (open circles); K_r 1 order of magnitude lower (crosses); K_c and K_r 1 order of magnitude higher (solid triangles); K_c and K_r 1 order of magnitude lower (open triangles). (b) Calculated versus measured ^{4}He concentrations for K_c and K_r 1 order of magnitude higher (solid triangles) and K_c and K_r 1 order of magnitude lower (open triangles). All parameters are the same as those of Figures 7b and 7c (calibrated 3-D groundwater transport model).

(see section 9.1) displays an almost perfect fit for TX02, with a deviation of −1.2% from the measured value. Calibration achieved for samples TX22 and TX32 are, at a first view, not as good, with deviations of −31.0 and −33.5%, respectively. It should be noted, however, that one additional He component not previously mentioned in this manuscript, an excess air component resulting from dissolution of small air bubbles caused by fluctuations of water table, is commonly present in groundwaters [*Heaton and Vogel*, 1981]. This excess air component, when present, can be significant in recharge areas where ^{4}He concentrations are mostly of atmospheric origin. With the exception of the recharge area, this excess air component is generally negligible in most groundwater samples.

[78] When conducting our transport model simulations, this excess air component is not taken into account, as the amount of such component, when present, varies randomly with sample location. Measured ^{4}He concentrations presented here correspond to the total measured concentration of the sample (Table 1). If one subtracts the excess air component from samples TX22 and TX32, a very good fit is obtained, with deviations between calculated and measured values of 3.0 and 8.8%, respectively. Such small deviations indicate that an excellent calibration for ^{4}He transport was achieved throughout the 3-D model not only in the confined portion of the Carrizo, but also in its recharge area.

9.6.2. Confined Portion of the Carrizo

[79] Despite simplifications inherent in the 3-D model as compared to the real system, agreement between most measured and calculated values is satisfactory. However, none of the simulations we carried out are able to reproduce concentrations in samples TX01, TX08, TX14, and TX24, and model parameters needed to arrive at measured concentrations are extreme. For example, calibrating TX08 and TX24 would require fluxes 23.8 and 27.2 times higher, respectively, than that obtained in our 3-D calibrated model. Alternatively, initial hydraulic conductivities in the Carrizo and Recklaw formations would have to be 20 times lower than calibrated values, and would be in contradiction with available field information [*Mace and Smyth*, 2003]. In addition, calibration of these four samples would make it impossible to achieve calibration for most of the samples located in the confined portion of the aquifer (80% of the total).

[80] In a thorough analysis of multiple helium components, *Castro et al.* [2000] show that these four samples present anomalous ^{4}He excesses as compared to the general trend exhibited by the entire data set. Although ^{4}He excess for TX01 is not readily explained, He component analysis for samples TX14 and TX24 [*Castro et al.*, 2000] suggests the presence of a strong upward leakage of ^{14}C-free water into the Carrizo, carrying additional ^{4}He. Compared to TX14 and TX24, TX08 exhibits a low ^{3}He/^{4}He ratio, suggesting that a local distinct in situ production rate might occur.

[81] TX01, TX08 and TX24 are located close to local faults that could provide a preferential pathway for vertical circulation of deeper waters toward the Carrizo aquifer. However, these faults are probably not hydrologically active, and such ^{4}He excess anomalies are not apparent deeper in the Carrizo aquifer. This suggests that recharge water may mix with localized inputs of older waters from deeper formations. Although ^{4}He excess observed at sample TX14 is not as pronounced as that in TX24, TX14 is located farther south of a local two-fault corridor and has already undergone dilution by the average ^{4}He concentrations present in the area.

9.7. Comparison of Calibrated 2-D and 3-D Model Results

[82] Comparison of the hydraulic conductivities derived from models in the Carrizo aquifer between 2-D [*Castro and Goblet*, 2003a] and 3-D model results (along plane 60) shows that 3-D model results are 1 to 2.5 times higher for most of the domain. Only locally do these values reach 3.5 times those obtained through 2-D simulations, and they are slightly lower (1−0.7 times) in a small area at the base of the Carrizo, at a distance between 25 and 57 km from the outcrop. Comparison of hydraulic conductivities in the Recklaw Formation show somewhat smaller discrepancies, with 3-D model results slightly lower than those in the 2-D simulations in the proximity of the outcrop area, and slightly higher deeper in the formation, to reach a maximum of 2.5 times greater than 2-D values. Overall, these discrepancies can be considered extremely minor taking into account that hydraulic conductivities vary over 13 orders of magnitude within different types of lithological facies. It further suggests that even though 2-D model simulations are unable to incorporate as much information as 3-D models, they remain suitable to reproduce regional groundwater flows systems, at least within the specific and more limited region represented in the 2-D model.

[83] Comparison of calculated ^{4}He concentrations between both models show minor deviations for most samples ($\ll$10%). The 2-D model results display ^{4}He concentrations at TX21 and TX25 that deviate +43.6 and −11.0%, respectively, from 3-D model results.

10. Conclusion

[84] In this paper, through the expansion of a previously built 2-D finite element model (adapted from *Castro and Goblet*, 2003a) into a 3-D one of the Carrizo aquifer and surrounding formations in southwestern Texas, we assess the ability of 2-D models to accurately represent water flow and ^{4}He transport in regional 3-D groundwater flow systems. We further assess the ability of 3-D models to provide a more detailed and accurate definition of the heterogeneities of the system, by specifically identifying and differentiating processes that directly impact the three-dimensional hydraulic conductivity field of a regional groundwater flow system. To this end, we developed a 3-D finite element model of the study area, which comprises mainly Atascosa, McMullen, Frio, and Live Oak counties. The 3-D model covers a surface area of ∼7000 km^2, and it includes 5,089,848 elements and 2,909,238 nodes.

[85] Through a step-by-step procedure it is shown that, in a similar manner to that of previous analytical and numerical models for the same area [*Castro et al.*, 2000; *Castro and Goblet*, 2003a], hydraulic conductivity decreases exponentially along the regional groundwater flow direction, both in the Carrizo and overlying confining layer. Simulations conducted with the 3-D model for water flow and

^{4}He transport show, however, that such exponential decrease is better described as a function of depth (along Z) rather than as a function of recharge distance [*Castro et al.*, 2000; *Castro and Goblet*, 2003a]. The established direct relationship between hydraulic conductivity-depth results mainly from differential compaction of the media and, to a lesser extent, from a change of lithological facies. Hydraulic conductivity decrease along Z is more pronounced in the eastern part of the domain, where the dip of the formations is more accentuated, and where compaction has likely played a more prominent role. In addition, our relationship intrinsic permeability-depth derived from the obtained hydraulic conductivity field in the 3-D model domain for depths $\leq$2 km is in agreement with that one proposed by *Saar and Manga* [2004] for the Oregon Cascades volcanic setting, as well as that proposed by *Manning and Ingebritsen* [1999]. These findings suggest that large-scale permeability evolves similarly with depth, independently of the type of medium. In addition, our ^{4}He calibrated 3-D flow model requires a simultaneous linear decrease of hydraulic conductivity along the Y direction, representing lateral changes in lithological facies present in the domain. Thus 3-D simulations allow for a more detailed and accurate definition of the heterogeneities of the system. This more accurate representation of the 3-D hydraulic conductivity field will in turn allow for a more accurate estimation of helium fluxes in the region by refining previous estimations of crustal and mantle helium components calculated through the original 2-D model (cf. *Castro*, 2004).

[86] As previously discussed by *Konikow and Bredehoeft* [1992], *Maloszewski and Zuber* [1993], *Castro and Goblet* [2003a], and others, 3-D simulations highlight once again the existence of an infinite number of solutions for regional groundwater flow models calibrated on measured hydraulic heads. Here, ^{4}He played a key role as an independent tracer, not only reducing the number of solutions available for calibration of the 3-D groundwater flow model but also highlighting the main factors directly impacting the three-dimensional hydraulic conductivity field of this real system.

[87] Calculated hydraulic conductivities vary from 5×10^{-4} to 3.1×10^{-8} m s^{-1} in the Carrizo aquifer from the outcrop to the discharge area. For the Recklaw Formation, corresponding values are 2.1×10^{-8} and 1.4×10^{-12} m s^{-1}, respectively. These values are in agreement with those found by *Castro and Goblet* [2003a]. In addition, our three-dimensional Carrizo hydraulic conductivity field displays values over the entire domain close to those obtained from field observations [*Mace and Smyth*, 2003]. The ^{4}He external flux value for which calibration of the 3-D transport model was achieved is 1.5×10^{-15} mol m$_{rock}^{-2}$ s^{-1}, a value that is 3.4 times lower than one obtained through an analytical model [*Castro et al.*, 2000] and almost 3 times greater than that one obtained by a 2-D finite element model [*Castro and Goblet*, 2003a].

[88] Comparison of 2-D [*Castro and Goblet*, 2003a] and our 3-D calibrated model results shows that, with a few local exceptions, 3-D model hydraulic conductivities in the Carrizo aquifer are 1 to 2.5 times higher for most of the domain. Comparison of the hydraulic conductivity field in the Recklaw Formation displays even smaller discrepancies, with 3-D model results slightly lower as compared to those obtained from the 2-D simulations at the proximity of the outcrop, and slightly higher deeper in the formation. Overall, these discrepancies can be considered minor, taking into account that hydraulic conductivities vary over 13 orders of magnitude within different types of lithological facies. This, in turn, further suggests that even though 2-D model simulations are unable to incorporate as much information as 3-D models, 2-D models remain suitable for reproducing regional groundwater flow systems, at least within the specific and more limited region represented by the 2-D model. Comparison of ^{4}He calculated concentrations between both models show minor deviations for most samples ($\ll$10%), further reinforcing our conclusions.

[89] **Acknowledgments.** The authors wish to thank L. F. Konikow, G. de Marsily, B. Wilkinson, and N. Jeannée for their insightful and constructive comments for improving the manuscript. The authors also thank F. Albarède and A. Revil for their constructive comments and editorial handling of this manuscript, as well as G. Garven and S. Ingebritsen for their insightful and thorough reviews which led to a much improved final version of this manuscript. We thank O. Stab for making available to us the Delos code, as well as E. T. Baker (USGS, Austin), R. E. Mace (Texas Water Development Board, Austin), and J.-P. Nicot (Bureau of Economic Geology, Austin) for their help in providing additional geological and hydrogeological information. Financial support by the U.S. National Science Foundation grant EAR-03087 07, the Elizabeth Caroline Crosby Research Award (NSF ADVANCE at the University of Michigan), and the "Ministère des Affaires Etrangères," France, for D. Patriarche through the program "Bourse Lavoisier", is greatly appreciated.

References

Alexander, W. H., Jr., and D. E. White (1966), Ground-water resources of Atascosa and Frio Counties, Texas, *Rep. 32*, 211 pp., Tex. Water Dev. Board, Austin.

Allegre, C. J., T. Staudacher, and P. Sarda (1987), Rare gas systematics; formation of the atmosphere, evolution and structure of the Earth's mantle, *Earth Planet. Sci. Lett.*, *81*(2–3), 127–150.

Anders, R. B. (1957), Ground-water geology of Wilson County, Texas, *Bull. 5710*, 62 pp., Tex. Board of Water Eng., Austin.

Anders, R. B. (1960), Ground-water geology of Karnes County, Texas, *Bull. 6007*, 107 pp., Tex. Board of Water Eng., Austin.

Anders, R. B., and E. T. Baker (1961), Ground-water geology of Live Oak County, Texas, *Bull. 6105*, 119 pp., Tex. Board of Water Eng., Austin.

Athy, L. F. (1930), Density, porosity, and compaction of sedimentary rocks, *Am. Assoc. Pet. Geol. Bull.*, *14*(1), 1–24.

Ballentine, C. J., R. K. O'Nions, E. R. Oxburgh, F. Horvath, and J. Deak (1991), Rare gas constraints on hydrocarbon accumulation, crustal degassing and groundwater flow in the Pannonian Basin, *Earth Planet. Sci. Lett.*, *105*(1–3), 229–246.

Bebout, D. G., V. J. Gavenda, A. R. Gregory, S. C. Claypool, J. H. Han, and J. H. Seo (1978), Geothermal resources, Wilcox Group, Texas Gulf Coast, *Rep. ORO/4891-3*, 82 pp., Bur. of Econ. Geol., Univ. of Tex. at Austin, Austin.

Bebout, D. G., B. R. Weise, A. R. Gregory, and M. B. Edwards (1982), Wilcox Sandstone reservoirs in the deep subsurface along the Texas Gulf Coast; their potential for production of geopressured geothermal energy, *Rep. Invest. 117*, 125 pp., Bur. of Econ. Geol., Univ. of Tex. at Austin, Austin.

Bitzer, K. (1999), Two-dimensional simulation of elastic and carbonate sedimentation, consolidation, subsidence, fluid flow, heat flow and solute transport during the formation of sedimentary basins, *Comput. Geosci.*, *25*(4), 431–447.

Bleines, C., J. Deraisme, F. Geffroy, N. Jeannée, S. Perseval, F. Rambert, D. Renard, and Y. Touffait (2002), *ISATIS Software Manual*, 645 pp., Géovariances, Fontainebleau, France.

Boisson, J. Y., L. Bertrand, J. F. Heitz, and Y. Moreau-Le Golvan (2001), In situ and laboratory investigations of fluid flow through an argillaceous formation at different scales of space and time, Tournemire tunnel, southern France, *Hydrogeol. J.*, *9*(1), 108–123.

Brace, W. F. (1984), Permeability of crystalline rocks; new in situ measurements, *J. Geophys. Res.*, *89*(B6), 4327–4330.

Bredehoeft, J. D., and S. S. Papadopulos (1980), A method for determining the hydraulic properties of tight formations, *Water Resour. Res.*, *16*(1), 233–238.

Bredehoeft, J. D., C. E. Neuzil, and P. C. D. Milly (1983), Regional flow in the Dakota Aquifer; a study of the role of confining layers, *U.S. Geol. Surv. Water Supply Pap., W 2237*, 45 pp.

Brinkman, J. E. (1981), Water age of the Carrizo sand, Ph.D. thesis, Univ. of Ariz., Tucson.

Carrera, J., and S. P. Neuman (1986), Estimation of aquifer parameters under transient and steady state conditions: 3. Application to synthetic and field data, *Water Resour. Res.*, *22*(2), 228–242.

Castro, M. C. (2004), Helium sources in passive margin aquifers - new evidence for a significant mantle ^{3}He source in aquifers with unexpectedly low in-situ ^{3}He/^{4}He production, *Earth Planet. Sci. Lett.*, *222*(3–4), 897–913.

Castro, M. C., and P. Goblet (2003a), Calibration of regional groundwater flow models: Working toward a better understanding of site-specific systems, *Water Resour. Res.*, *39*(6), 1172, doi:10.1029/2002WR001653.

Castro, M. C., and P. Goblet (2003b), Noble gas thermometry and hydrologic ages: Evidence for late Holocene warming in southwest Texas, *Geophys. Res. Lett.*, *30*(24), 2251, doi:10.1029/2003GL018875.

Castro, M. C., A. Jambon, G. de Marsily, and P. Schlosser (1998a), Noble gases as natural tracers of water circulation in the Paris Basin: 1. Measurements and discussion of their origin and mechanisms of vertical transport in the basin, *Water Resour. Res.*, *34*(10), 2443–2466.

Castro, M. C., P. Goblet, E. Ledoux, S. Violette, and G. de Marsily (1998b), Noble gases as natural tracers of water circulation in the Paris Basin: 2. Calibration of a groundwater flow model using noble gas isotope data, *Water Resour. Res.*, *34*(10), 2467–2483.

Castro, M. C., M. Stute, and P. Schlosser (2000), Comparison of the ^{4}He ages and ^{14}C ages in simple aquifer systems: Implications for groundwater flow and chronologies, *Appl. Geochem.*, *15*, 1137–1167.

Connolly, C. A., L. M. Walter, H. Baadsgaard, and F. J. Longstaffe (1990), Origin and evolution of formation waters, Alberta Basin, western Canada sedimentary basin; I, Chemistry, *Appl. Geochem.*, *5*(4), 375–395.

Cordier, E., and P. Goblet (1999), Programme METIS—Simulation d'écoulement et de transport miscible en milieu poreux et fracturé, *Notice Emploi LHM/RD/99/18*, Cent. d'Inf. Géol., Ecole Natl. Supér. des Mines de Paris, Fontainebleau, France.

Craig, H., J. E. Lupton, and Y. Horibe (1978), A mantle helium component in Circum-Pacific volcanic gases; Hakone, the Marianas, and Mt. Lassen, in *Terrestrial Rare Gases*, edited by E. C. Alexander Jr. and M. Ozima, pp. 3–16, Jpn. Sci. Soc. Press, Tokyo.

Davis, J. C. (2002), *Statistics and Data Analysis in Geology*, 638 pp., John Wiley, New York.

de Marsily, G. (1986), *Quantitative Hydrogeology*, 440 pp., Academic, San Diego, Calif.

de Marsily, G., J. P. Delhomme, A. Coudrain-Ribstein, and M. Lavenue (2000), Four decades of inverse problems in hydrogeology, in *Theory, Modeling, and Field Investigation in Hydrogeology: A Special Volume in Honor of Shlomo P. Neuman's 60th Birthday*, edited by D. Zhang and C. L. Winter, pp. 1–17, Geol. Soc. of Am., Boulder, Colo.

de Marsily, G., J. Gonçalves, S. Violette, and M. C. Castro (2002), Migration mechanisms of radionuclides from a clay repository toward adjacent aquifers and the surface, *C. R. Acad. Sci. Phys.*, *3*(7–8), 945–959.

Desbarats, A. J., M. J. Hinton, C. E. Logan, D. R. Sharpe, and V. Remenda (2001), Geostatistical mapping of leakance in a regional aquitard, Oak Ridges Moraine area, Ontario, Canada, *Hydrogeol. J.*, *9*(1), 79–96.

Farley, K. A., and E. Neroda (1998), Noble gases in the Earth's mantle, *Annu. Rev. Earth Planet. Sci.*, *26*, 189–218.

Fisher, W. L. (1969), Gulf Coast Basin tertiary delta systems, in *Delta Systems in Exploration for Oil and Gas*, edited by W. L. Fisher, pp. 3–90, Bur. of Econ. Geol., Univ. of Tex. at Austin, Austin.

Fogg, G. E. (1986), Groundwater flow and sand body interconnectedness in a thick, multiple-aquifer system, *Water Resour. Res.*, *22*(5), 679–694.

Freeze, R. A., and J. A. Cherry (1979), *Groundwater*, 604 pp., Prentice-Hall, Old Tappan, N. J.

Galloway, W. E., T. E. Ewing, C. M. Garrett, N. Tyler, and D. G. Bebout (1983), Atlas of major Texas oil reservoirs, report, Bur. of Econ. Geol., Austin, Tex.

Gangi, A. F. (1978), Variation of whole and fractured porous rock permeability with confining pressure, *Int. J. Rock Mech. Min. Sci. Geomech. Abstr.*, *15*(5), 249–257.

Gouze, P., and A. Coudrain-Ribstein (2002), Chemical reactions and porosity changes during sedimentary diagenesis, *Appl. Geochem.*, *17*(1), 39–47.

Hamlin, H. S. (1988), Depositional and ground-water flow systems of the Carrizo-Upper Wilcox, south Texas, *Rep. Invest. 175*, 61 pp., Bur. of Econ. Geol., Austin, Tex.

Harris, H. B. (1965), Ground-water resources of La Salle and McMullen counties, Texas, *Bull. 6520*, 96 pp., Tex. Water Commission, Austin.

Harvey, C. F., and S. M. Gorelick (1995), Mapping hydraulic conductivity; sequential conditioning with measurements of solute arrival time, hydraulic head, and local conductivity, *Water Resour. Res.*, *31*(7), 1615–1626.

Heaton, T. H. E., and J. C. Vogel (1981), "Excess air" in groundwater, *J. Hydrol.*, *50*(1–4), 201–216.

Ingebritsen, S. E., R. H. Mariner, and D. R. Sherrod (1994), Hydrothermal systems of the Cascade Range, north-central Oregon, *U.S. Geol. Surv. Prof. Pap., 1044-L*.

Kitanidis, P. K. (1993), Generalized covariance functions in estimation, *Math. Geol.*, *25*(5), 525–540.

Kitanidis, P. K. (1999), Generalized covariance functions associated with the Laplace equation and their use in interpolation and inverse problems, *Water Resour. Res.*, *35*(5), 1361–1367.

Klemt, W. B., G. L. Duffin, and G. R. Elder (1976), Ground-water resources of the Carrizo Aquifer in the Winter Garden area of Texas, vol. I, *Rep. 210(1)*, 30 pp., Tex. Water Dev. Board, Austin.

Koltermann, C. E., and S. M. Gorelick (1996), Heterogeneity in sedimentary deposits: A review of structure-imitating, process-imitating, and descriptive approaches, *Water Resour. Res.*, *32*(9), 2617–2658.

Konikow, L. F., and J. D. Bredehoeft (1992), Ground-water models cannot be validated, *Adv. Water Resour.*, *15*(1), 75–83.

Kosters, E. C., and R. J. Finley (1989), Atlas of major Texas gas reservoirs, report, Bur. of Econ. Geol., Austin, Tex.

Land, L. S., K. L. Milliken, and E. F. McBride (1987), Diagenetic evolution of Cenozoic sandstones, Gulf of Mexico sedimentary basin, *Sediment. Geol.*, *50*(1–3), 195–225.

Lavenue, M., and J. Pickens (1992), Application of a coupled adjoint sensitivity and kriging approach to calibrate a groundwater flow, *Water Resour. Res.*, *28*(6), 1543–1569.

Le Gallo, Y., O. Bildstein, and E. Brosse (1998), Coupled reaction-flow modeling of diagenetic changes in reservoir permeability, porosity and mineral compositions, *J. Hydrol.*, *209*(1–4), 366–388.

Lonsdale, J. T. (1935), Geology and ground-water resources of Atascosa and Frio Counties, Texas, *U.S. Geol. Surv. Water Supply Pap., 676*, 90 pp.

Mace, R. E., and R. C. Smyth (2003), Hydraulic properties of the Carrizo-Wilcox aquifer in Texas: Information for groundwater modeling, planning, and management, *Rep. Invest. 269*, 40 pp., Univ. of Tex. at Austin, Bur. of Econ. Geol., New Orleans, La.

Maloszewski, P., and A. Zuber (1993), Principles and practice of calibration and validation of mathematical models for the interpretation of environmental tracer data in aquifers, *Adv. Water Resour.*, *16*(3), 173–190.

Manga, M. (1998), Advective heat transport by low-temperature discharge in the Oregon Cascades, *Geology*, *26*(9), 799–802.

Manning, C. E., and S. E. Ingebritsen (1999), Permeability of the continental crust: Implications of geothermal data and metamorphic systems, *Rev. Geophys.*, *37*(1), 127–150.

Martel, D. J., J. Deak, P. Dovenyi, F. Horvath, R. K. O'Nions, E. R. Oxburgh, L. Stegena, and M. Stute (1989), Leakage of helium from the Pannonian Basin, *Nature*, *342*(6252), 908–912.

Matheron, G. (1973), The intrinsic random functions and their applications, *Adv. Appl. Probab.*, *5*(1), 439–468.

Morrow, C., D. Lockner, S. Hickman, M. Rusanov, and T. Roeckel (1994), Effects of lithology and depth on the permeability of core samples from the Kola and KTB drillholes, *J. Geophys. Res.*, *99*(B4), 7263–7274.

Murray, G. E. (1955), Midway Stage, Sabine Stage and Wilcox Group, *Am. Assoc. Pet. Geol. Bull.*, *39*(5), 671–689.

Neuzil, C. E. (1994), How permeable are clays and shales?, *Water Resour. Res.*, *30*(2), 145–150.

O'Nions, R. K., and E. R. Oxburgh (1983), Heat and helium in the Earth, *Nature*, *306*(5942), 429–431.

Payne, J. N. (1972a), Geohydrologic significance of lithofacies of the Carrizo sand of Arkansas, Louisiana, and Texas and the Meridian sand of Mississippi, *U.S. Geol. Surv. Prof. Pap., 569-D*, 15 pp.

Payne, J. N. (1972b), Hydrologic significance of lithofacies of the Cane River Formation or equivalents in Arkansas, Louisiana, Mississippi and Texas, *U.S. Geol. Surv. Prof. Pap., 569-C*, 21 pp.

Pearson, F. J., Jr. (1966), Ground-water ages and flow rates by the carbon-14 method, Ph.D. thesis, Univ. of Tex. at Austin, Austin.

Phillips, F. M., and M. C. Castro (2003), Groundwater dating and residence-time measurements, in *Surface and Ground Water, Weathering, and Soils*, edited by J. I. Drever, pp. 451–497, Elsevier Sci., New York.

Revil, A., and L. M. Cathles (2002), Fluid transport by solitary waves along growing faults—A field example from the South Eugene Island Basin, Gulf of Mexico, *Earth Planet. Sci. Lett.*, *202*(2), 321–335.

Riggs, S. R., S. P. Ellison Jr., W. L. Fisher, W. E. Galloway, M. L. W. Jackson, and R. A. Morton (1991), Mineral resources and geopressure-geothermal energy, in *The Gulf of Mexico Basin*, edited by A. Salvador, pp. 495–528, Geol. Soc. of Am., Boulder, Colo.

Rowan, E. L., D. O. Hayba, P. H. Nelson, W. M. Burns, and D. W. Houseknecht (2003), Sandstone and shale compaction curves derived from sonic and gamma ray logs in offshore wells, North Slope, Alaska—Parameters for basin modeling, *U.S. Geol. Surv. Open File Rep., 03–0329*. (Available at http://geopubs.wr.usgs.gov/open-file/of03-329/)

Saar, M. O., and M. Manga (2004), Depth dependence of permeability in the Oregon Cascades inferred from hydrogeologic, thermal, seismic, and magmatic modeling constraints, *J. Geophys. Res.*, *109*(B4), B04204, doi:10.1029/2003JB002855.

Slaughter, G. M., R. M. White, and R. P. Alger (1983), Permeability of selected sediments in the vicinity of five salt domes in the gulf interior region, *Tech. Rep. 356*, 67 pp., Off. of Nucl. Waste-Isolation, Battelle Mem. Inst., Marietta, Ga.

Smith, L., and F. W. Schwartz (1981), Mass transport: 2. Analysis of uncertainty in prediction, *Water Resour. Res.*, *17*(2), 351–369.

Stab, O. (1995), La librairie DELOS—Notice de conception, Ecole Natl. Supér. des Mines de Paris, Fontainebleau, France.

Stute, M., P. Schlosser, J. F. Clark, and W. S. Broecker (1992), Paleotemperatures in the southwestern United States derived from noble gases in ground water, *Science*, *256*(5059), 1000–1001.

Terzaghi, K., and R. B. Peck (1967), *Soil Mechanics in Engineering Practice*, 729 pp., John Wiley, New York.

Torgersen, T., and W. B. Clarke (1985), Helium accumulation in groundwater, I: An evaluation of sources and the flux of crustal ^{4}He in the Great Artesian Basin, *Geochim. Cosmochim. Acta*, *49*(5), 1211–1218.

Torgersen, T., and J. O'Donnell (1991), The degassing flux from the solid earth: Release by fracturing, *Geophys. Res. Lett.*, *18*(5), 951–954.

Tóth, J. (1995), Hydraulic continuity in large sedimentary basins, *Hydrogeol. J.*, *3*(4), 4–16.

Turner, S. F. (1936), Wilson County, Texas, Records of wells, drillers' logs, and water analyses, and map showing location of wells, pp. 73, State Board of Water Eng., Austin, Tex.

Wei, H. F., E. Ledoux, and G. de Marsily (1990), Regional modelling of groundwater flow and salt and environmental tracer transport in deep aquifers in the Paris Basin, *J. Hydrol.*, *120*(1–4), 341–358.

Wierenga, P. J., R. G. Hills, and D. B. Hudson (1991), The Las-Cruces trench site: Characterization, experimental results, and one-dimensional flow predictions, *Water Resour. Res.*, *27*(10), 2695–2705.

M. C. Castro and D. Patriarche, Department of Geological Sciences, University of Michigan, 2534 C. C. Little Building, Ann Arbor, MI 48109-1063, USA. (mccastro@umich.edu; delfpat@umich.edu)

P. Goblet, Ecole des Mines de Paris, Centre d'Informatique Géologique, UMR 7619 SISYPHE, F-77305 Fontainebleau, France. (patrick.goblet@ensmp.fr)